
PROJECTING U.S. COASTAL STORM SURGE RISKS AND IMPACTS WITH DEEP LEARNING

PREPRINT

Julian R. Rice* **Karthik Balaguru** **Fadia Ticona Rollano** **John Wilson**
Brent Daniel **David Judi** **Ning Sun** **L. Ruby Leung**
Pacific Northwest National Laboratory
902 Battelle Boulevard, Richland, WA

June 18, 2025

ABSTRACT

Storm surge is one of the deadliest hazards posed by tropical cyclones (TCs), yet assessing its current and future risk is difficult due to the phenomenon's rarity and physical complexity. Recent advances in artificial intelligence applications to natural hazard modeling suggest a new avenue for addressing this problem. We utilize a deep learning storm surge model to efficiently estimate coastal surge risk in the United States from 900,000 synthetic TC events, accounting for projected changes in TC behavior and sea levels. The derived historical 100-year surge (the event with a 1% yearly exceedance probability) agrees well with historical observations and other modeling techniques. When coupled with an inundation model, we find that heightened TC intensities and sea levels by the end of the century result in a 50% increase in population at risk. Key findings include markedly heightened risk in Florida, and critical thresholds identified in Georgia and South Carolina.

1 Introduction

Tropical cyclones (TCs, also known as hurricanes or typhoons) have been the most damaging single form of weather-related natural disaster globally in terms of both loss of life and economic damage in recent decades (World Meteorological Organization, 2021). In the United States (U.S.), storm surge has been the leading cause of deaths directly attributable to TCs, making up nearly as many deaths as all other TC-induced hazards combined (Rappaport, 2014). With the growing density of people and assets in coastal regions (Klotzbach et al., 2018), paired with increasing TC intensities in the future (Knutson et al., 2020), the threat posed by TC-induced storm surge may only grow more pronounced. However, deadly storm surge is such a rare occurrence that the historical record is not an accurate measure of the true risk—and certainly does not capture the potential for future changes in TC behavior. While flood risk is most often communicated in terms of the 100-year (1% yearly exceedance probability) flood, such as in the Federal Emergency Management Agency (FEMA) Flood Insurance Rate Maps, the record of reliable surge observations in the U.S. is at most 150 years (generously, 1880–present (Needham, 2014)). Analyzing the 100-year event as a Bernoulli process suggests that the true 100-year return level has never been met or exceeded in this historical window for 22% of the U.S. coastline.

Given insufficient observational records, the other avenue to understanding future storm surge risk is via modeling. While simple parametric models of storm surge exist (Irish et al., 2008; Islam et al., 2021), the physical complexity of the processes involved render them incapable of sufficiently accurate spatial modeling. Physical-numerical models such as the Advanced Circulation (ADCIRC) model (Luettich et al., 1992; Pringle et al., 2021), Delft3D (Roelvink & Van Banning, 1995), the Finite-Volume Coastal Ocean Model (FVCOM) (Chen et al., 2003), and the Regional Ocean Model (ROMS) (Shchepetkin & McWilliams, 2005) are capable of highly accurate storm surge (and in some cases inland inundation) modeling. Yet, this accuracy requires a tradeoff with computational efficiency; due to the complex physics involved, these models often simulate fluid dynamics on the timescale of seconds on detailed meshes with many thousands of nodes. The computational expense associated with simulating thousands of years of TC activity are

*Corresponding author: julian.rice@pnnl.gov

thus immense, and usually preclude a Monte Carlo-style probabilistic uncertainty analysis. Only in the last handful of years have data-driven models (namely, deep neural networks) presented a viable alternative to numerical modeling approaches, as illustrated by recent advances in neural networks for global weather forecasting (Pathak et al., 2022; Bi et al., 2023; Lam et al., 2023; Price et al., 2024) and general circulation modeling (Kochkov et al., 2024), often with orders-of-magnitude speedups in prediction time. Theoretical analysis of these data-driven models indicates that sufficient training and model complexity allows them to implicitly encode the underlying physics of these systems (Rupe et al., 2022).

Previous deep learning approaches to storm surge modeling have shown promise, though these past methods have all been spatially inflexible either by training a model for only a single bay or subregion (Sztobryn, 2003; Lee, 2006; Oliveira et al., 2009; Hashemi et al., 2016; Sahoo & Bhaskaran, 2019; Lee et al., 2021; Xie et al., 2023; Adeli et al., 2023) or by training separate models for each location of interest (Lockwood et al., 2022) thereby foregoing the benefits of learning shared physics. In contrast, we propose a “point-based” approach, which enables our model to be highly flexible, parallelizable, and capable of learning more complete and generalized physics of storm surge across all locations. Our proposed model, which we call DeepSurge, is a recurrent neural network trained to predict the peak surge level at any given location in the North Atlantic basin, trained and validated on ADCIRC outputs from more than 250 historical TC storm surge events. Although by no means a perfect surrogate for ADCIRC, DeepSurge achieves reasonably skillful out-of-sample accuracy (81.5% R^2 , 0.25 m mean absolute error) and up to a 96x speedup in prediction time compared with ADCIRC. Further, DeepSurge and ADCIRC show comparable skill when validated against independent National Oceanic and Atmospheric Administration (NOAA) tide gauge observations.

For a robust quantification of risk, many thousands of TCs are required, necessitating the use of synthetic TC events. For this task, we use the Risk Analysis Framework for Tropical Cyclones (RAFT) (Xu et al., 2024) to generate 900,000 TCs ($\sim 60,000$ simulation years) representative of historical and future conditions, to our knowledge an order of magnitude larger than any previous synthetic TC-driven storm surge risk assessment. From these storms, we use DeepSurge to robustly estimate surge heights along the entire U.S. Gulf and Atlantic coastline, and combine with probabilistic sea-level rise projections and an efficient inland inundation model to characterize the extremes of storm surge flooding risk impacts.

2 Methods

2.1 Numerical storm surge simulations

A large and varied dataset of historical storm surge data was generated with the ADCIRC model (Luettich Jr. & Westerink, 1991; Luettich et al., 1992; Pringle et al., 2021), utilizing a mesh of 15,467 nodes spanning the North Atlantic basin. Historical TC data for the North Atlantic was retrieved from the International Best Track Archive for Climate Stewardship (IBTrACS) (Knapp et al., 2010, 2018). Wind forcings were generated with the method described in Emanuel & Rotunno (2011), and pressure forcing with the methodology presented by Holland (2008). Simulations were run at 1-second time steps for the lifetime of each storm, with the maximum water level at each node retained as the training target for our deep learning surrogate model. Further details are provided in Supplementary Section 1.

2.2 DeepSurge, a deep learning storm surge model

We develop a neural network model informed by the physics of the problem, which we call DeepSurge. Because storm surge is the result of complex physical interactions in space (coastal geometry and bathymetry) and time (storm evolution), our model utilizes both convolutional and recurrent neural network components which are known to be skilled in processing these forms of data respectively (O’Shea & Nash, 2015; Hochreiter & Schmidhuber, 1997) and have been successfully utilized in previous storm surge modeling approaches (Adeli et al., 2023; Xie et al., 2023; Giaremis et al., 2024). Our model differs from others in that it operates in a “point-based” manner, meaning it processes each node independently from its neighbors, which allows more flexibility, generalizability, and parallelization than previous approaches. The DeepSurge model ingests a timeseries and spatial maps describing a single node during a storm, and predicts that node’s maximum surge level.

The basic structure of the neural network, as detailed in Figure 1, has four stages: 1) encode the timeseries and spatial data separately, 2) convert them to compatible shapes and concatenate them together, 3) apply a Long Short-Term Memory (LSTM) (Hochreiter & Schmidhuber, 1997) layer to understand the temporal development, and 4) decode the features to predict a maximum surge level. The timeseries input to the model consists of a wide variety of variables describing the time evolution of the storm and its relation to the node of interest: storm maximum wind speed, storm radius of maximum wind, distance from node of interest to storm center, direction from node of interest to storm center, storm translation speed, and direction of storm motion. Also included are a few time-invariant scalars: bathymetric

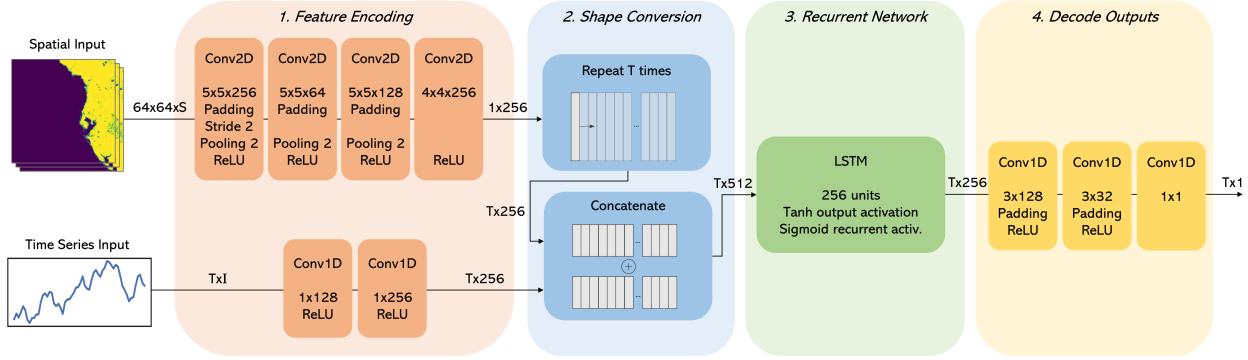


Figure 1: DeepSurge architecture. Tensor shapes (batch size not included) are given for each arrow, representing that tensor being passed from one layer to the next. In the tensor shapes, S is the number of spatial images, T is the number of timesteps, and I is the number of timeseries inputs. Convolutions are summarized with kernel size K and number of filters F , e.g. $K \times K \times F$ for a 2D convolution

depth at the node of interest and estimated slope and direction of the seafloor. All directions and angles are encoded as sine/cosine pairs to avoid discontinuities. The spatial inputs to the model consist of a log-scaled bathymetric map interpolated from the ADCIRC mesh, and a land-ocean mask derived from 300-m resolution European Space Agency global land cover data (European Space Agency, 2017). Both are 128x128 pixel grids at 0.0222° resolution centered on the node of interest, resulting in roughly a 300 km diameter receptive field. The network is constructed and trained in TensorFlow/Keras (Martín Abadi et al., 2015), and has a total of 1.7 million parameters. Details of the architecture and training methodology are provided in Supplementary Section 2.2.

2.3 Validation & sensitivity analysis of deep learning method

DeepSurge demonstrates promising generalization skill on the test set, which consists of 71 storms that the model has never been trained or tuned on. When compared to the corresponding ADCIRC simulations, DeepSurge achieves an 81.5% R^2 score, a mean squared error of 0.224 m, and a mean absolute error of 0.258 m in predicting peak surge heights per node. We additionally perform a validation against NOAA tide gauge observations². Although tide gauges are quite accurate under normal conditions, they often fail or malfunction during extreme surge events, which causes weaker events to be sampled more reliably than stronger ones. Overall, DeepSurge shows reasonable skill in capturing these gauge-observed surge peaks, with error metrics ($R^2 = 0.403$, MAE = 0.474m, RMSE = 0.664m) similar to the ADCIRC simulations ($R^2 = 0.427$, MAE = 0.543m, RMSE = 0.882m), and highly significant Pearson and Spearman correlations ($p \ll 0.001$). Possibly due to the negative sampling bias of the gauge observations, both DeepSurge and ADCIRC exhibit similar positive mean biases (+0.217m and +0.203m respectively). Sensitivity analysis suggests this bias may affect estimated inundation totals on the order of 14-18%. See Supplementary Section 2.4 for further details of the tide gauge comparison and sensitivity analysis.

2.4 Quantifying storm surge risk with synthetic tropical cyclones

Synthetic tropical cyclones are generated with the the Risk Analysis Framework for Tropical Cyclones (RAFT) (Xu et al., 2021; Balaguru et al., 2023; Xu et al., 2024), forced by the climate conditions from nine Coupled Model Intercomparison Project Phase 6 (CMIP6) general circulation models (GCMs). The RAFT synthetic TC method produces realistic and diverse synthetic TC geneses, tracks, and intensities (Xu et al., 2024), and has been used in past studies to assess changes in TC landfall frequency (Balaguru et al., 2023), wind turbine damage (Lipari et al., 2024), and power outage risk (Rice et al., 2025). RAFT is forced with the climate conditions from a historical (1980–2014) and end-of-century future (2066–2100) period under Shared Socioeconomic Pathway SSP5-8.5 from nine CMIP6 models. We generate 50,000 TCs from the forcings of each of the 18 CMIP6 model-time period pairs, for a total of 900,000 tracks. Quantile delta mapping (Cannon et al., 2015) is applied to the TC intensities to correct for biases in the CMIP6 forcings. The set of synthetic TCs used in this study are identical to those described in and utilized by Lipari et al. (2024) and Rice et al. (2025). For further details on these synthetic storms, see those publications and Supplementary Section 1.

²Accessible from the Tides & Currents API: <https://api.tidesandcurrents.noaa.gov/mdapi/prod/#>

For each of these storms, DeepSurge is used to predict peak storm surge levels at 1,100 points along the U.S. Gulf and Atlantic coast. Projected surge levels in the future period are combined with the probabilistic sea-level rise projections from Kopp et al. (2014) to create a joint probability distribution at every coastal location. As in other studies (Gori et al., 2022), surge and sea-level rise are treated as linearly additive, and the future distributions of TC climatology and sea-level rise as independent (which may result in generally conservative estimates of future change (Little et al., 2015)).

2.5 CA-Surge, a simple inland inundation model

Lastly, we evaluate the impacts of modeled extreme water levels with a simple and efficient inundation model, CA-Surge, which puts projected changes in terms of the number of people impacted and enables analysis of sensitivity to various sources of uncertainty. CA-Surge is a “bathtub-style” model similar to previously published approaches (Strauss et al., 2012; Yunus et al., 2016; Williams & Lück-Vogel, 2020) with the addition of an overland attenuation factor, which accounts for the reduction of surge height as water moves inland due to bottom friction. Attenuation rates are gathered from Vafeidis et al. (2019), though it should be noted that there is substantial uncertainty inherent in attenuation rate estimates. Inundated areas are combined with LandScan (Dobson et al., 2000) night-time population maps for estimates of affected population (for interpretability, we hold population constant between the historical and future periods). This method is found to produce reasonable estimates of inundated area compared with observations from Hurricane Katrina and captures state-level patterns in populations at risk from the 100-year coastal flood as derived by FEMA (see Supplementary Section 3.2). Still, we stress that this is an approximate method, useful primarily for efficient assessment of large-scale surge inundation. Pseudo-code of the CA-Surge algorithm is provided in Supplementary Section 3.1.

3 Results

The combination of RAFT, DeepSurge, and CA-Surge makes tractable the efficient simulation of many thousands of storm events, which enables robust estimation of the effect of changes in TC behavior on once-in-a-century coastal flood extremes. In this section, we evaluate the historical 100-year surge heights, analyze how they are projected to change in the future, and then put these changes in terms of population at risk of flooding.

3.1 Extreme storm surge heights

The ensemble median 100-year surge event as modeled by our method for the historical period (Fig. 2a) shows predictable patterns. The highest surges occur primarily in the Gulf Coast where landfalling major hurricanes are most common, with peaks clustered in bays and concave coastlines. From the east coast of Florida and northward along the Atlantic, the combination of a steeper continental shelf and fewer major hurricanes results in lower extremes, with notable exceptions in areas with more complex coastal geometries including the Chesapeake Bay, Delaware Bay, and Long Island Sound. However, the results in the Chesapeake Bay appear to be anomalous; we find that this outlier is inherited from the original ADCIRC simulations, which had insufficient spatial resolution to resolve the fine-scale riverine and estuarine hydrodynamic processes in this region. Addressing this issue is planned for future work. Results in the Maryland-Virginia region are provided in this remainder of this work for completeness but should be treated with caution due to these biases. Otherwise, the spatial pattern of our modeled 100-year event appears qualitatively reasonable.

To quantitatively verify that the combination of DeepSurge and RAFT are producing accurate 100-year surge heights, we compare our ensemble median return levels with the historical 100-year event observational estimates from Needham (2014), who undertook an exhaustive analysis of the historical storm surge record 1900–2014 throughout the Gulf of Mexico, and three of independent surge modeling techniques: Gori et al. (2022) applied ADCIRC to a similar synthetic TC model forced with NCEP reanalysis; Muis et al. (2023) forced the Global Tide and Surge Model (a hydrodynamic model based on Delft3D) with historical ERA5 reanalysis; and lastly, for a comparison with a simple parametric model we generate surges with the Storm Surge Hazard Potential Index (SSHPI) developed by Islam et al. (2021), forced by the same RAFT synthetic TCs as DeepSurge. We find that our method matches the observed distribution of 100-year surge heights at least as well as the other modeling methods, and shows strong and statistically significant correlation with the patterns produced by them (Spearman correlations ≥ 0.5 , $p < 0.05$; see Supplementary Section 2.5 for details). DeepSurge achieves this comparable level of skill while being much more computationally efficient than numerical hydrodynamic models (up to 96x faster than our ADCIRC configuration; see Supplementary Section 2.3).

In the future period, RAFT projects broadly increasing coastal TC intensities, with the 100-year storm intensity increasing in strength by roughly one Saffir-Simpson category in most coastal regions (Supplementary Fig. 1). The synthetic TCs also move slower on average in the future period, with slight differences in storm movement direction

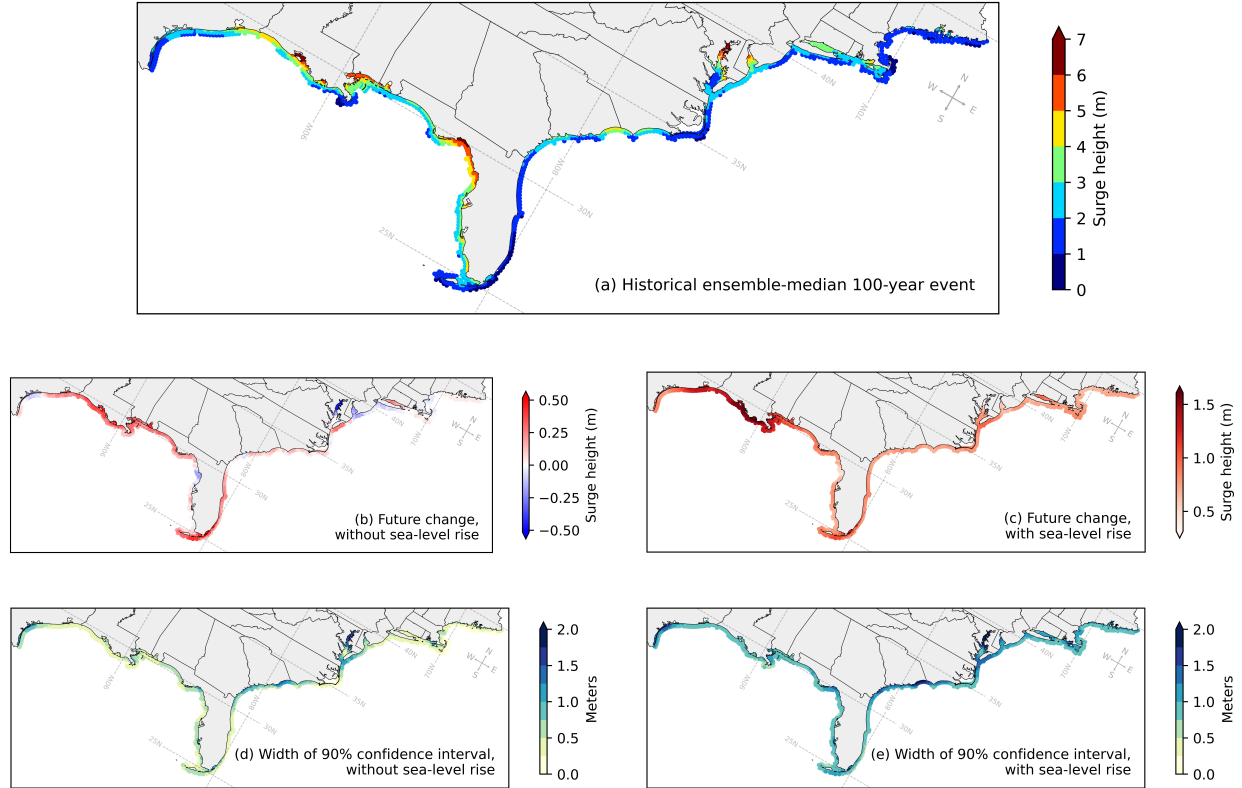


Figure 2: (a) DeepSurge modeled historical ensemble-median 100-year event; the corresponding future change (b) with and (c) without sea-level rise; and respective widths of the 90% confidence intervals (d,e).

most visible in the vicinity of Florida (Supplementary Fig. 2). These differences in TC behavior cause substantial changes in storm surge as modeled by DeepSurge. Even without sea-level rise, the model indicates that these differences in TC behavior will produce notably larger 100-year surge levels across the northern Gulf Coast and eastern Florida (up to +78 cm), with more heterogeneous results for the rest of the coastline (Fig. 2b). These results are in broad agreement with past studies such as Gori et al. (2022). Causal analysis suggests that the increase in future TC intensities is the dominant factor contributing to these changes, while decreasing storm translation speeds are generally a weakly negative factor (Supplementary Section 4). The westward shift in average storm direction in the vicinity of Florida (Supplementary Fig. 2) may explain the differing responses on the peninsula’s eastern and western coasts despite similar increases in TC intensities. Overall, altered TC behavior is projected to be a positive factor, increasing surge height by an average of +8.4 cm.

The inclusion of sea-level rise (Fig. 2c) results in much larger changes, with a mean increase of +85 cm and maximum of +170 cm relative to historical, though with correspondingly larger uncertainty (Fig. 2e). While the effect of sea-level rise is generally larger than that of future TC behavior (roughly two times larger at the peak along the Louisiana coast), the latter is still a significant contributor especially in capturing differences across finer spatial scales.

3.2 Changing coastal inundation risk

While the quantification of future changes in extreme surge heights is of vital importance, it lacks crucial context; due to widely varying topographies and population densities, the relationship between surge height and flood damage on the U.S. coast is spatially variable and non-linear. Thus, to translate our projected surge heights into human impacts, we use CA-Surge, a simple bathtub-style inundation model with an overland frictional attenuation effect (as described in the Methods section). Note that since the CA-Surge model is only an approximation of true inundation physics, more emphasis should be placed on relative changes than on absolute totals.

Even under historical climate conditions, the flooding risk posed by the 100-year storm surge event is significant—with an estimated 4.6 million people at risk—yet this risk is substantially heightened in our projected future scenario (Fig.

3). Similar to the changes in surge heights, future changes in inundation risk are driven primarily by sea level rise (+1.9 million people at risk above historical; Fig. 3c) with changes in future TC behavior being a secondary contributor (+0.24 million people at risk above historical; Fig. 3b). Taken together, risk is projected to increase in every coastal state (Fig. 3d), with a 50% increase in population at risk overall (+2.3 million people above historical). Florida alone projects to see an additional roughly one million residents at risk in the future period, as it sees one of the larger state-level relative increases in risk on top of its already large historical risk.

Crucially, the percentage change in inundation risk at a state level is not always proportional to the local increase in 100-year surge height. While the largest future changes in surge height were observed in the central Gulf states of Louisiana, Alabama, and Mississippi, relative changes in coastal flood risk are most concentrated along the southeast Atlantic coast. For example, although Georgia and South Carolina see relatively moderate increases in 100-year surge heights in the future compared to many other states (Fig. 2c), they have among the largest percentage increases in inundation risk (Fig. 3d). This suggests that these states' coastal topographies may exhibit critical thresholds, above which population centers currently insulated from risk may become rapidly more vulnerable. This hypothesis is explored in Figure 4, which plots the relationship between average coastal surge height and population at risk for Georgia and South Carolina, with Alabama as a counterexample. Around the two meter threshold of coastal surge height, Georgia and South Carolina's risk curves inflect upward sharply, while Alabama's remains fairly linear. Thus, despite Alabama exhibiting a much larger future change in surge height on top of an already higher baseline 100-year surge, Georgia and South Carolina experience larger increases (in both absolute and percentage terms) in population at risk. These drastic differences in risk curve slope indicate that any future increase in surge height for Georgia and South Carolina is much more damaging than the same increase in Alabama would be. This finding underscores the importance of framing storm surge projections in terms of inundation risk instead of surge height, as these impactful nonlinear relationships would otherwise be missed.

The large sample size of synthetic TC events and ensemble forcings allow for robust uncertainty quantification as well, which also exhibits nonlinear and heterogeneous patterns. The spatial distribution of uncertainty (Supplementary Fig. 3)—arising from the combination of uncertainties in GCM-induced TC behavior and sea-level rise—varies widely, with some states seeing proportionally much wider 90% uncertainty bounds than others (e.g., New York vs. Louisiana), or greatly increasing uncertainty in the future (e.g., Florida). Beyond the 90% bounds, the tails of the distributions tend to be much longer in the future than in the historical period, due to long tails in the sea-level rise projections (Supplementary Fig. 4). Very generally, uncertainty in population at risk from the 100-year event appears to be lower in the Gulf, and larger along the Atlantic coast.

4 Discussion

This study couples an ensemble of global projections of future ocean-atmospheric conditions, a synthetic TC model, a novel deep learning storm surge model, and an efficient inland inundation model to assess changes in storm surge risk and associated flooding impacts for the U.S. coastline. With an unprecedented sample size of TC events, we find substantial ($\sim 50\%$) increases in population at risk of once-in-a-century surge flooding, and characterize the spatial pattern and variability of this risk. While increases in 100-year surge heights are most prominent along the Gulf Coast, the pattern of inundation risk (as modulated by coastal topography and population densities) is revealed to be much more variable, exhibiting complex and non-linear interactions.

Our deep learning storm surge model, DeepSurge, is not a replacement for numerical storm surge models but serves as a useful complement to them, particularly in situations where traditional models may pose an intolerable computational cost or throughput. While this study demonstrates the utility of such a deep learning storm surge model in assessing surge risk, the technique is still evolving, and—like all data-driven methods—is inherently limited by the quality and scope of its training data. Given that the model operates on individual points rather than a fixed mesh, we intend to explore assimilating additional data from diverse regional and high-resolution hydrodynamic models during the training process. This may help address known biases in complex regions such as the Chesapeake Bay, where resolving fine-scale dynamics remains challenging. A similar technique may further allow the expansion of our model to new basins and domains across the globe.

While accurately projecting flood risk is important on its own, continuing study is needed to further out understanding of the broader socioeconomic impacts of flooding. Beyond the immediate threats to wellbeing, floods cause a wide range of adverse and long-lasting effects, including increased disease and mortality (Alderman et al., 2012; Stephens et al., 2007), mental health disruptions (Graham et al., 2019; Alderman et al., 2012), and unemployment (Allaire, 2018; Peek-Asa et al., 2012). Complex and varied patterns in the socioeconomic effects of flooding emerge across different coastal regions (Montgomery & Chakraborty, 2013; Maldonado et al., 2016; Qiang, 2019; Herreros-Cantis et al., 2020; Smiley et al., 2022), particularly in its impacts to housing and home valuations (Varela Varela, 2023; Zhang, 2016;

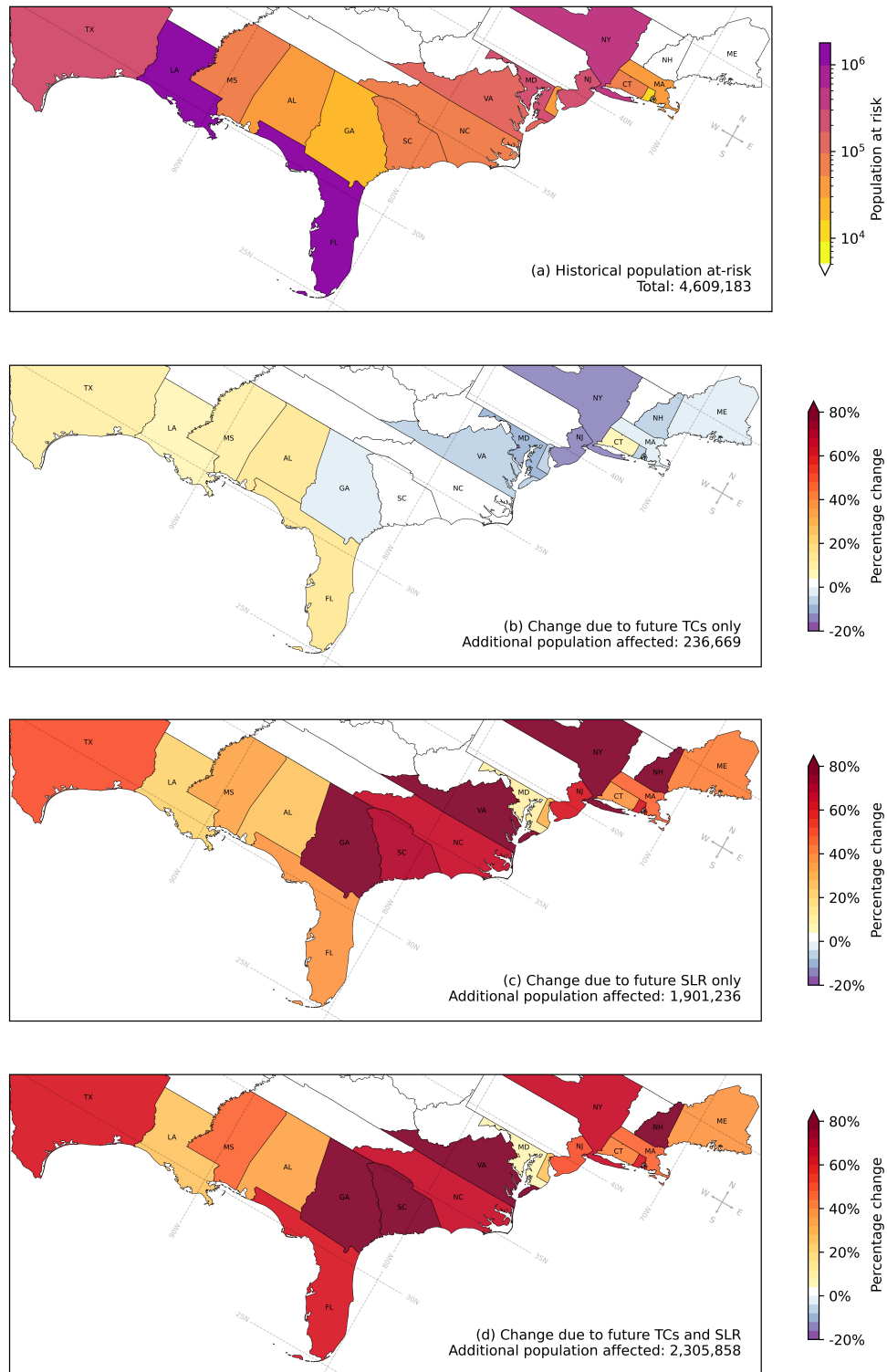


Figure 3: Modeled population at risk from the 100-year flood event in (a) the historical period, and the percentage change in the future period with (b) future TCs only, (c) future sea-level rise (SLR) only, and (d) the combination of the two. All panels show the ensemble median estimate.

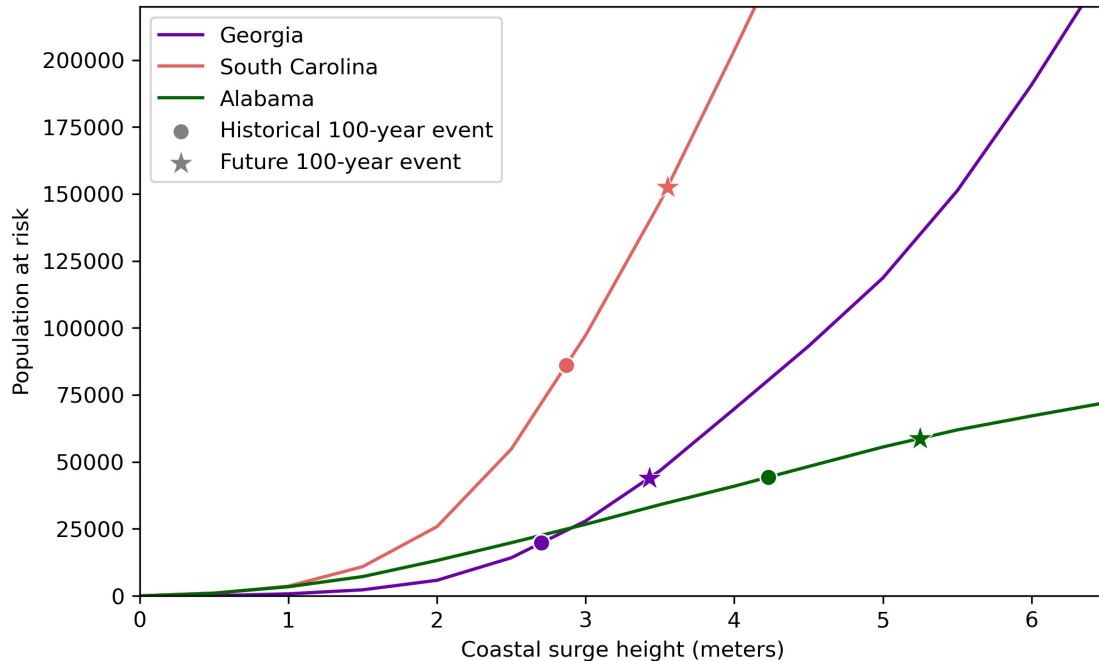


Figure 4: Curves relating average coastal surge height to population at risk for three selected states. The rapid steepening of Georgia and South Carolina’s risk curves leads to large future changes in inundation risk, despite these states having both a lower historical 100-year surge height and a smaller absolute change in future surge height than states such as Alabama.

Van der Straten, 2023; Billings et al., 2022). Given these ramifications, careful consideration of adaption, mitigation, and retreat strategies at local and national scales is essential (Neumann et al., 2015).

Acknowledgments

This work was supported by the Multisector Dynamics and Regional and Global Model Analysis program areas of the U.S. Department of Energy (DOE), Office of Science, Office of Biological and Environmental Research as part of the multi-program, collaborative Integrated Coastal Modeling (ICoM) project. The Pacific Northwest National Laboratory is operated for DOE by Battelle Memorial Institute under contract DE-AC05-76RL01830.

This research used resources of the National Energy Research Scientific Computing Center (NERSC), a U.S. Department of Energy Office of Science User Facility located at Lawrence Berkeley National Laboratory, operated under Contract No. DE-AC02-05CH11231 using NERSC award BER-ERCAP0024320. This work also used the computing resources of Pacific Northwest National Lab’s Institutional Computing facility.

Data Availability

DeepSurge-predicted storm surge heights for all 900,000 synthetic storm tracks are made publicly available on Zenodo: <https://doi.org/10.5281/zenodo.15021868>. All other data sources used in this study are publicly available, as is the ADCIRC algorithm.

References

Adeli, E., Sun, L., Wang, J., and Taflanidis, A. A. An advanced spatio-temporal convolutional recurrent neural network for storm surge predictions. *Neural Computing and Applications*, 35(26):18971–18987, September 2023. ISSN 1433-3058. doi:10.1007/s00521-023-08719-2. URL <https://doi.org/10.1007/s00521-023-08719-2>.

- Alderman, K., Turner, L. R., and Tong, S. Floods and human health: A systematic review. *Environment International*, 47: 37–47, October 2012. ISSN 0160-4120. doi:10.1016/j.envint.2012.06.003. URL <https://www.sciencedirect.com/science/article/pii/S0160412012001237>.
- Allaire, M. Socio-economic impacts of flooding: A review of the empirical literature. *Water Security*, 3:18–26, May 2018. ISSN 2468-3124. doi:10.1016/j.wasec.2018.09.002. URL <https://www.sciencedirect.com/science/article/pii/S2468312418300063>.
- Balaguru, K., Xu, W., Chang, C.-C., Leung, L. R., Judi, D. R., Hagos, S. M., Wehner, M. F., Kossin, J. P., and Ting, M. Increased U.S. coastal hurricane risk under climate change. *Science Advances*, 9(14):eadf0259, April 2023. doi:10.1126/sciadv.adf0259. URL <https://www.science.org/doi/full/10.1126/sciadv.adf0259>. Publisher: American Association for the Advancement of Science.
- Bi, K., Xie, L., Zhang, H., Chen, X., Gu, X., and Tian, Q. Accurate medium-range global weather forecasting with 3D neural networks. *Nature*, 619(7970):533–538, July 2023. ISSN 1476-4687. doi:10.1038/s41586-023-06185-3. URL <https://www.nature.com/articles/s41586-023-06185-3>. Publisher: Nature Publishing Group.
- Billings, S. B., Gallagher, E. A., and Ricketts, L. Let the rich be flooded: The distribution of financial aid and distress after hurricane harvey. *Journal of Financial Economics*, 146(2):797–819, November 2022. ISSN 0304-405X. doi:10.1016/j.jfineco.2021.11.006. URL <https://www.sciencedirect.com/science/article/pii/S0304405X21005067>.
- Cannon, A. J., Sobie, S. R., and Murdock, T. Q. Bias Correction of GCM Precipitation by Quantile Mapping: How Well Do Methods Preserve Changes in Quantiles and Extremes? *Journal of Climate*, 28(17):6938–6959, September 2015. ISSN 0894-8755, 1520-0442. doi:10.1175/JCLI-D-14-00754.1. URL <https://journals.ametsoc.org/view/journals/clim/28/17/jcli-d-14-00754.1.xml>. Publisher: American Meteorological Society Section: Journal of Climate.
- Chen, C., Liu, H., and Beardsley, R. C. An unstructured grid, finite-volume, three-dimensional, primitive equations ocean model: application to coastal ocean and estuaries. *Journal of atmospheric and oceanic technology*, 20(1): 159–186, 2003.
- Dobson, J. E., Bright, E. A., Coleman, P. R., Durfee, R. C., and Worley, B. A. LandScan: a global population database for estimating populations at risk. *Photogrammetric Engineering & Remote Sensing*, 66(7), 2000. doi:10.1201/9781482264678-24. URL <https://www.taylorfrancis.com/books/9781482264678/chapters/10.1201/9781482264678-24>.
- Emanuel, K. and Rotunno, R. Self-Stratification of Tropical Cyclone Outflow. Part I: Implications for Storm Structure. *Journal of the Atmospheric Sciences*, 68(10):2236–2249, October 2011. ISSN 0022-4928, 1520-0469. doi:10.1175/JAS-D-10-05024.1.
- European Space Agency. Land Cover CCI Product User Guide Version 2. Tech. Rep., 2017. URL maps.elie.ucl.ac.be/CCI/viewer/download/ESACCI-LC-Ph2-PUGv2_2.0.pdf.
- Giaremis, S., Nader, N., Dawson, C., Kaiser, H., Kaiser, C., and Nikidis, E. Storm Surge Modeling in the AI ERA: Using LSTM-based Machine Learning for Enhancing Forecasting Accuracy, March 2024. URL <http://arxiv.org/abs/2403.04818>. arXiv:2403.04818 [physics].
- Gori, A., Lin, N., Xi, D., and Emanuel, K. Tropical cyclone climatology change greatly exacerbates US extreme rainfall–surge hazard. *Nature Climate Change*, 12(2):171–178, February 2022. ISSN 1758-6798. doi:10.1038/s41558-021-01272-7. URL <https://www.nature.com/articles/s41558-021-01272-7>. Publisher: Nature Publishing Group.
- Graham, H., White, P., Cotton, J., and McManus, S. Flood- and Weather-Damaged Homes and Mental Health: An Analysis Using England’s Mental Health Survey. *International Journal of Environmental Research and Public Health*, 16(18):3256, January 2019. ISSN 1660-4601. doi:10.3390/ijerph16183256. URL <https://www.mdpi.com/1660-4601/16/18/3256>. Number: 18 Publisher: Multidisciplinary Digital Publishing Institute.
- Hashemi, M. R., Spaulding, M. L., Shaw, A., Farhadi, H., and Lewis, M. An efficient artificial intelligence model for prediction of tropical storm surge. *Natural Hazards*, 82(1):471–491, May 2016. ISSN 1573-0840. doi:10.1007/s11069-016-2193-4. URL <https://doi.org/10.1007/s11069-016-2193-4>.
- Herreros-Cantis, P., Olivotto, V., Grabowski, Z. J., and McPhearson, T. Shifting landscapes of coastal flood risk: environmental (in)justice of urban change, sea level rise, and differential vulnerability in New York City. *Urban Transformations*, 2(1):9, July 2020. ISSN 2524-8162. doi:10.1186/s42854-020-00014-w. URL <https://doi.org/10.1186/s42854-020-00014-w>.
- Hochreiter, S. and Schmidhuber, J. Long short-term memory. *Neural computation*, 9(8):1735–1780, 1997. Publisher: MIT press.

- Holland, G. A Revised Hurricane Pressure–Wind Model. *Monthly Weather Review*, 136, September 2008. doi:10.1175/2008MWR2395.1. URL <https://journals.ametsoc.org/view/journals/mwre/136/9/2008mwr2395.1.xml>.
- Irish, J. L., Resio, D. T., and Ratcliff, J. J. The Influence of Storm Size on Hurricane Surge. *Journal of Physical Oceanography*, 38(9):2003–2013, September 2008. ISSN 0022-3670, 1520-0485. doi:10.1175/2008JPO3727.1. URL <https://journals.ametsoc.org/view/journals/phoc/38/9/2008jpo3727.1.xml>. Publisher: American Meteorological Society Section: Journal of Physical Oceanography.
- Islam, M. R., Lee, C.-Y., Mandli, K. T., and Takagi, H. A new tropical cyclone surge index incorporating the effects of coastal geometry, bathymetry and storm information. *Scientific Reports*, 11(1):16747, August 2021. ISSN 2045-2322. doi:10.1038/s41598-021-95825-7. URL <https://www.nature.com/articles/s41598-021-95825-7>. Number: 1 Publisher: Nature Publishing Group.
- Klotzbach, P. J., Bowen, S. G., Pielke, R., and Bell, M. Continental U.S. Hurricane Landfall Frequency and Associated Damage: Observations and Future Risks. *Bulletin of the American Meteorological Society*, 99(7):1359–1376, July 2018. ISSN 0003-0007, 1520-0477. doi:10.1175/BAMS-D-17-0184.1. URL <https://journals.ametsoc.org/view/journals/bams/99/7/bams-d-17-0184.1.xml>. Publisher: American Meteorological Society Section: Bulletin of the American Meteorological Society.
- Knapp, K. R., Kruk, M. C., Levinson, D. H., Diamond, H. J., and Neumann, C. J. The International Best Track Archive for Climate Stewardship (IBTrACS): Unifying Tropical Cyclone Data. *Bulletin of the American Meteorological Society*, 91(3):363–376, March 2010. ISSN 0003-0007, 1520-0477. doi:10.1175/2009BAMS2755.1. URL https://journals.ametsoc.org/view/journals/bams/91/3/2009bams2755_1.xml. Publisher: American Meteorological Society Section: Bulletin of the American Meteorological Society.
- Knapp, K. R., Diamond, H. J., Kossin, J. P., Kruk, M. C., and Schreck, C. J. International Best Track Archive for Climate Stewardship (IBTrACS) Project, Version 4, North Atlantic, 2018.
- Knutson, T., Camargo, S. J., Chan, J. C. L., Emanuel, K., Ho, C.-H., Kossin, J., Mohapatra, M., Satoh, M., Sugi, M., Walsh, K., and Wu, L. Tropical Cyclones and Climate Change Assessment: Part II: Projected Response to Anthropogenic Warming. *Bulletin of the American Meteorological Society*, 101(3):E303–E322, March 2020. ISSN 0003-0007, 1520-0477. doi:10.1175/BAMS-D-18-0194.1. URL <https://journals.ametsoc.org/view/journals/bams/101/3/bams-d-18-0194.1.xml>. Publisher: American Meteorological Society Section: Bulletin of the American Meteorological Society.
- Kochkov, D., Yuval, J., Langmore, I., Norgaard, P., Smith, J., Mooers, G., Klöwer, M., Lottes, J., Rasp, S., Düben, P., Hatfield, S., Battaglia, P., Sanchez-Gonzalez, A., Willson, M., Brenner, M. P., and Hoyer, S. Neural general circulation models for weather and climate. *Nature*, 632(8027):1060–1066, August 2024. ISSN 1476-4687. doi:10.1038/s41586-024-07744-y. URL <https://www.nature.com/articles/s41586-024-07744-y>. Publisher: Nature Publishing Group.
- Kopp, R. E., Horton, R. M., Little, C. M., Mitrovica, J. X., Oppenheimer, M., Rasmussen, D. J., Strauss, B. H., and Tebaldi, C. Probabilistic 21st and 22nd century sea-level projections at a global network of tide-gauge sites. *Earth's Future*, 2(8):383–406, 2014. ISSN 2328-4277. doi:10.1002/2014EF000239. URL <https://onlinelibrary.wiley.com/doi/abs/10.1002/2014EF000239>. _eprint: <https://onlinelibrary.wiley.com/doi/pdf/10.1002/2014EF000239>.
- Lam, R., Sanchez-Gonzalez, A., Willson, M., Wirnsberger, P., Fortunato, M., Alet, F., Ravuri, S., Ewalds, T., Eaton-Rosen, Z., Hu, W., Merose, A., Hoyer, S., Holland, G., Vinyals, O., Stott, J., Pritzel, A., Mohamed, S., and Battaglia, P. Learning skillful medium-range global weather forecasting. *Science*, 382(6677):1416–1421, December 2023. doi:10.1126/science.adi2336. URL <https://www.science.org/doi/10.1126/science.adi2336>. Publisher: American Association for the Advancement of Science.
- Lee, J.-W., Irish, J. L., Bensi, M. T., and Marcy, D. C. Rapid prediction of peak storm surge from tropical cyclone track time series using machine learning. *Coastal Engineering*, 170:104024, December 2021. ISSN 0378-3839. doi:10.1016/j.coastaleng.2021.104024. URL <https://www.sciencedirect.com/science/article/pii/S0378383921001691>.
- Lee, T.-L. Neural network prediction of a storm surge. *Ocean Engineering*, 33(3):483–494, March 2006. ISSN 0029-8018. doi:10.1016/j.oceaneng.2005.04.012. URL <https://www.sciencedirect.com/science/article/pii/S002980180500140X>.
- Lipari, S., Balaguru, K., Rice, J., Feng, S., Xu, W., K. Berg, L., and Judi, D. Amplified threat of tropical cyclones to US offshore wind energy in a changing climate. *Communications Earth & Environment*, 5(1):1–10, December 2024. ISSN 2662-4435. doi:10.1038/s43247-024-01887-6. URL <https://www.nature.com/articles/s43247-024-01887-6>. Publisher: Nature Publishing Group.

- Little, C. M., Horton, R. M., Kopp, R. E., Oppenheimer, M., Vecchi, G. A., and Villarini, G. Joint projections of US East Coast sea level and storm surge. *Nature Climate Change*, 5(12):1114–1120, December 2015. ISSN 1758-6798. doi:10.1038/nclimate2801. URL <https://www.nature.com/articles/nclimate2801>. Publisher: Nature Publishing Group.
- Lockwood, J. W., Lin, N., Oppenheimer, M., and Lai, C.-Y. Using Neural Networks to Predict Hurricane Storm Surge and to Assess the Sensitivity of Surge to Storm Characteristics. *Journal of Geophysical Research: Atmospheres*, 127(24):e2022JD037617, 2022. ISSN 2169-8996. doi:10.1029/2022JD037617. URL <https://onlinelibrary.wiley.com/doi/abs/10.1029/2022JD037617>. _eprint: <https://onlinelibrary.wiley.com/doi/pdf/10.1029/2022JD037617>.
- Luetlich, R. A., Westerink, J. J., and Scheffner, N. W. ADCIRC: an advanced three-dimensional circulation model for shelves, coasts, and estuaries. Report 1, Theory and methodology of ADCIRC-2DD1 and ADCIRC-3DL. 1992. Publisher: Coastal Engineering Research Center (US).
- Luetlich Jr., R. A. and Westerink, J. J. A solution for the vertical variation of stress, rather than velocity, in a three-dimensional circulation model. *International Journal for Numerical Methods in Fluids*, 12(10):911–928, 1991. ISSN 1097-0363. doi:10.1002/flid.1650121002.
- Maldonado, A., Collins, T. W., Grineski, S. E., and Chakraborty, J. Exposure to Flood Hazards in Miami and Houston: Are Hispanic Immigrants at Greater Risk than Other Social Groups? *International Journal of Environmental Research and Public Health*, 13(8):775, August 2016. ISSN 1660-4601. doi:10.3390/ijerph13080775. URL <https://www.mdpi.com/1660-4601/13/8/775>. Number: 8 Publisher: Multidisciplinary Digital Publishing Institute.
- Martín Abadi, Ashish Agarwal, Paul Barham, Eugene Brevdo, Zhifeng Chen, Craig Citro, Greg S. Corrado, Andy Davis, Jeffrey Dean, Matthieu Devin, Sanjay Ghemawat, Ian Goodfellow, Andrew Harp, Geoffrey Irving, Michael Isard, Jia, Y., Rafal Jozefowicz, Lukasz Kaiser, Manjunath Kudlur, Josh Levenberg, Dandelion Mané, Rajat Monga, Sherry Moore, Derek Murray, Chris Olah, Mike Schuster, Jonathon Shlens, Benoit Steiner, Ilya Sutskever, Kunal Talwar, Paul Tucker, Vincent Vanhoucke, Vijay Vasudevan, Fernanda Viégas, Oriol Vinyals, Pete Warden, Martin Wattenberg, Martin Wicke, Yuan Yu, and Xiaoqiang Zheng. TensorFlow: Large-Scale Machine Learning on Heterogeneous Systems, 2015. URL <https://www.tensorflow.org/>.
- Montgomery, M. C. and Chakraborty, J. Social Vulnerability to Coastal and Inland Flood Hazards: A Comparison of GIS-Based Spatial Interpolation Methods. *International Journal of Applied Geospatial Research (IJAGR)*, 4(3):58–79, July 2013. ISSN 1947-9654. doi:10.4018/jagr.2013070104. URL <https://www.igi-global.com/article/content/www.igi-global.com/article/content/77925>. Publisher: IGI Global.
- Muis, S., Aerts, J. C. J. H., Á. Antolínez, J. A., Dullaart, J. C., Duong, T. M., Erikson, L., Haarsma, R. J., Apecechea, M. I., Mengel, M., Le Bars, D., O’Neill, A., Ranasinghe, R., Roberts, M. J., Verlaan, M., Ward, P. J., and Yan, K. Global Projections of Storm Surges Using High-Resolution CMIP6 Climate Models. *Earth’s Future*, 11(9): e2023EF003479, 2023. ISSN 2328-4277. doi:10.1029/2023EF003479. URL <https://onlinelibrary.wiley.com/doi/abs/10.1029/2023EF003479>. _eprint: <https://onlinelibrary.wiley.com/doi/pdf/10.1029/2023EF003479>.
- Needham, H. *A Data-Driven Storm Surge Analysis for the U.S. Gulf Coast*. Doctor of Philosophy, Louisiana State University and Agricultural and Mechanical College, March 2014. URL https://repository.lsu.edu/gradschool_dissertations/3250.
- Neumann, J. E., Emanuel, K., Ravela, S., Ludwig, L., Kirshen, P., Bosma, K., and Martinich, J. Joint effects of storm surge and sea-level rise on US Coasts: new economic estimates of impacts, adaptation, and benefits of mitigation policy. *Climatic Change*, 129(1):337–349, March 2015. ISSN 1573-1480. doi:10.1007/s10584-014-1304-z. URL <https://doi.org/10.1007/s10584-014-1304-z>.
- Oliveira, M. M. F. d., Ebecken, N. F. F., Oliveira, J. L. F. d., and Santos, I. d. A. Neural Network Model to Predict a Storm Surge. *Journal of Applied Meteorology and Climatology*, 48(1):143–155, January 2009. ISSN 1558-8424, 1558-8432. doi:10.1175/2008JAMC1907.1. URL <https://journals.ametsoc.org/view/journals/apme/48/1/2008jamc1907.1.xml>. Publisher: American Meteorological Society Section: Journal of Applied Meteorology and Climatology.
- O’Shea, K. and Nash, R. An introduction to convolutional neural networks. *arXiv preprint arXiv:1511.08458*, 2015.
- Pathak, J., Subramanian, S., Harrington, P., Raja, S., Chattopadhyay, A., Mardani, M., Kurth, T., Hall, D., Li, Z., Aizzadenesheli, K., Hassanzadeh, P., Kashinath, K., and Anandkumar, A. FourCastNet: A Global Data-driven High-resolution Weather Model using Adaptive Fourier Neural Operators, February 2022. URL <http://arxiv.org/abs/2202.11214>. arXiv:2202.11214.

- Peek-Asa, C., Ramirez, M., Young, T., and Cao, Y. Flood-Related Work Disruption and Poor Health Outcomes Among University Students. *Prehospital and Disaster Medicine*, 27(6):503–508, December 2012. ISSN 1049-023X, 1945-1938. doi:10.1017/S1049023X1200129X. URL <https://www.cambridge.org/core/journals/prehospital-and-disaster-medicine/article/abs/floodrelated-work-disruption-and-poor-health-outcomes-among-university-students/656ED60550A6B7B719003C908B70CAF6>.
- Price, I., Sanchez-Gonzalez, A., Alet, F., Andersson, T. R., El-Kadi, A., Masters, D., Ewalds, T., Stott, J., Mohamed, S., Battaglia, P., Lam, R., and Willson, M. GenCast: Diffusion-based ensemble forecasting for medium-range weather, May 2024. URL <http://arxiv.org/abs/2312.15796>. arXiv:2312.15796.
- Pringle, W. J., Wirasaet, D., Roberts, K. J., and Westerink, J. J. Global storm tide modeling with ADCIRC v55: unstructured mesh design and performance. *Geoscientific Model Development*, 14(2):1125–1145, February 2021. ISSN 1991-959X. doi:10.5194/gmd-14-1125-2021. URL <https://gmd.copernicus.org/articles/14/1125/2021/>. Publisher: Copernicus GmbH.
- Qiang, Y. Disparities of population exposed to flood hazards in the United States. *Journal of Environmental Management*, 232:295–304, February 2019. ISSN 0301-4797. doi:10.1016/j.jenvman.2018.11.039. URL <https://www.sciencedirect.com/science/article/pii/S0301479718313057>.
- Rappaport, E. N. Fatalities in the United States from Atlantic Tropical Cyclones: New Data and Interpretation. *Bulletin of the American Meteorological Society*, 95(3):341–346, March 2014. ISSN 0003-0007, 1520-0477. doi:10.1175/BAMS-D-12-00074.1. URL <https://journals.ametsoc.org/view/journals/bams/95/3/bams-d-12-00074.1.xml>. Publisher: American Meteorological Society Section: Bulletin of the American Meteorological Society.
- Rice, J. R., Balaguru, K., Staid, A., Xu, W., and Judi, D. Projected increases in tropical cyclone-induced U.S. electric power outage risk. *Environmental Research Letters*, 20(3):034030, February 2025. ISSN 1748-9326. doi:10.1088/1748-9326/adad85. URL <https://dx.doi.org/10.1088/1748-9326/adad85>. Publisher: IOP Publishing.
- Roelvink, J. and Van Banning, G. Design and development of DELFT3D and application to coastal morphodynamics. *Oceanographic Literature Review*, 11(42):925, 1995.
- Rupe, A., Vesselinov, V., and Crutchfield, J. P. Nonequilibrium statistical mechanics and optimal prediction of partially-observed complex systems. *New Journal of Physics*, May 2022.
- Sahoo, B. and Bhaskaran, P. K. Prediction of storm surge and inundation using climatological datasets for the Indian coast using soft computing techniques. *Soft Computing*, 23(23):12363–12383, December 2019. ISSN 1433-7479. doi:10.1007/s00500-019-03775-0. URL <https://doi.org/10.1007/s00500-019-03775-0>.
- Shchepetkin, A. F. and McWilliams, J. C. The regional oceanic modeling system (ROMS): a split-explicit, free-surface, topography-following-coordinate oceanic model. *Ocean Modelling*, 9(4):347–404, January 2005. ISSN 1463-5003. doi:10.1016/j.ocemod.2004.08.002. URL <https://www.sciencedirect.com/science/article/pii/S1463500304000484>.
- Smiley, K. T., Noy, I., Wehner, M. F., Frame, D., Sampson, C. C., and Wing, O. E. J. Social inequalities in climate change-attributed impacts of Hurricane Harvey. *Nature Communications*, 13(1):3418, August 2022. ISSN 2041-1723. doi:10.1038/s41467-022-31056-2. URL <https://www.nature.com/articles/s41467-022-31056-2>. Publisher: Nature Publishing Group.
- Stephens, K. U., Grew, D., Chin, K., Kadetz, P., Greenough, P. G., Burkle, F. M., Robinson, S. L., and Franklin, E. R. Excess mortality in the aftermath of Hurricane Katrina: a preliminary report. *Disaster Medicine and Public Health Preparedness*, 1(1):15–20, July 2007. ISSN 1938-744X. doi:10.1097/DMP.0b013e3180691856.
- Strauss, B. H., Ziemiński, R., Weiss, J. L., and Overpeck, J. T. Tidally adjusted estimates of topographic vulnerability to sea level rise and flooding for the contiguous United States. *Environmental Research Letters*, 7(1):014033, March 2012. ISSN 1748-9326. doi:10.1088/1748-9326/7/1/014033. URL <https://dx.doi.org/10.1088/1748-9326/7/1/014033>. Publisher: IOP Publishing.
- Sztobryn, M. Forecast of storm surge by means of artificial neural network. *Journal of Sea Research*, 49(4):317–322, June 2003. ISSN 1385-1101. doi:10.1016/S1385-1101(03)00024-8. URL <https://www.sciencedirect.com/science/article/pii/S1385110103000248>.
- Vafeidis, A. T., Schuerch, M., Wolff, C., Spencer, T., Merkens, J. L., Hinkel, J., Lincke, D., Brown, S., and Nicholls, R. J. Water-level attenuation in global-scale assessments of exposure to coastal flooding: a sensitivity analysis. *Natural Hazards and Earth System Sciences*, 19(5):973–984, May 2019. ISSN 1561-8633. doi:10.5194/nhess-19-973-2019. URL <https://nhess.copernicus.org/articles/19/973/2019/>. Publisher: Copernicus GmbH.

- Van der Straten, Y. Flooded House or Underwater Mortgage? The Macrofinancial Implications of Climate Change and Adaptation, March 2023. URL <https://papers.ssrn.com/abstract=4393731>.
- Varela Varela, A. Surge of Inequality: How Different Neighborhoods React to Flooding. *SSRN Electronic Journal*, 2023. ISSN 1556-5068. doi:10.2139/ssrn.4396481. URL <https://www.ssrn.com/abstract=4396481>.
- Williams, L. L. and Lück-Vogel, M. Comparative assessment of the GIS based bathtub model and an enhanced bathtub model for coastal inundation. *Journal of Coastal Conservation*, 24(2):23, March 2020. ISSN 1874-7841. doi:10.1007/s11852-020-00735-x. URL <https://doi.org/10.1007/s11852-020-00735-x>.
- World Meteorological Organization. *WMO Atlas of Mortality and Economic Losses from Weather, Climate and Water Extremes (1970–2019)*, volume WMO-No. 1267 of *WMO*. WMO, Geneva, 2021. ISBN 978-92-63-11267-5.
- Xie, W., Xu, G., Zhang, H., and Dong, C. Developing a deep learning-based storm surge forecasting model. *Ocean Modelling*, 182:102179, April 2023. ISSN 1463-5003. doi:10.1016/j.ocemod.2023.102179. URL <https://www.sciencedirect.com/science/article/pii/S1463500323000203>.
- Xu, W., Balaguru, K., August, A., Lalo, N., Hodas, N., DeMaria, M., and Judi, D. Deep Learning Experiments for Tropical Cyclone Intensity Forecasts. *Weather and Forecasting*, 36(4):1453–1470, August 2021. ISSN 1520-0434, 0882-8156. doi:10.1175/WAF-D-20-0104.1. URL <https://journals.ametsoc.org/view/journals/wefo/36/4/WAF-D-20-0104.1.xml>. Publisher: American Meteorological Society Section: Weather and Forecasting.
- Xu, W., Balaguru, K., Judi, D. R., Rice, J., Leung, L. R., and Lipari, S. A North Atlantic synthetic tropical cyclone track, intensity, and rainfall dataset. *Scientific Data*, 11(1):130, January 2024. ISSN 2052-4463. doi:10.1038/s41597-024-02952-7. URL <https://www.nature.com/articles/s41597-024-02952-7>. Number: 1 Publisher: Nature Publishing Group.
- Yunus, A. P., Avtar, R., Kraines, S., Yamamuro, M., Lindberg, F., and Grimmond, C. S. B. Uncertainties in Tidally Adjusted Estimates of Sea Level Rise Flooding (Bathtub Model) for the Greater London. *Remote Sensing*, 8(5): 366, May 2016. ISSN 2072-4292. doi:10.3390/rs8050366. URL <https://www.mdpi.com/2072-4292/8/5/366>. Number: 5 Publisher: Multidisciplinary Digital Publishing Institute.
- Zhang, L. Flood hazards impact on neighborhood house prices: A spatial quantile regression analysis. *Regional Science and Urban Economics*, 60:12–19, September 2016. ISSN 0166-0462. doi:10.1016/j.regsciurbeco.2016.06.005. URL <https://www.sciencedirect.com/science/article/pii/S0166046216300540>.

Supplementary Information for “Projecting U.S. coastal storm surge risks and impacts with deep learning”

Julian R. Rice^{1,*}, Karthik Balaguru¹, Fadia Ticona Rollano¹, John Wilson¹, Brent Daniel¹, David Judi¹, Ning Sun¹, and L. Ruby Leung¹

¹Pacific Northwest National Laboratory

*Corresponding author: julian.rice@pnnl.gov

S1 RAFT synthetic tropical cyclones

The Risk Analysis Framework for Tropical Cyclones (RAFT) (Xu et al., 2021; Balaguru et al., 2023; Xu et al., 2024) is a synthetic TC downscaling method. It uses a random seeding process for cyclogenesis conditioned on historical observations, with a physical beta-advection model for track propagation (Emanuel et al., 2006; Marks, 1992; Kelly et al., 2018) and a deep learning regressor to model 6-hourly intensity changes over the lifetime of a storm (Xu et al., 2021). Radius of maximum wind is parameterized with a log-transformed linear regression on latitude and maximum wind speed, following Willoughby et al. (2006). Since large uncertainties remain about the rate of TC genesis in the future (Knutson et al., 2020; Murakami & Wang, 2022; Chavas et al., 2024), we use a fixed rate of 14.91 seeds per year (the observed historical rate in IBTrACS from 1980-2014) for both the historical and future periods. Note that the intensity model quickly dissipates or sustains TC seeds depending on how favorable their environment is, which allows the climate to implicitly regulate TC frequency.

Climate conditions are gathered for the historical (1980–2014) and end-of-century future (2066–2100) periods under Shared Socioeconomic Pathway SSP5-8.5 from nine CMIP6 models: the Euro-Mediterranean Centre on Climate Change coupled climate model (CMCC-CM2-SR5), Canadian Earth System Model (CanESM5), Energy Exascale Earth System Model (E3SM), EC-Earth Consortium Model (EC-Earth3), Geophysical Fluid Dynamics Laboratory Climate Model (GFDLCM4), Institute Pierre Simon Laplace Climate Model (IPSL-CM6A-LR), Model for Interdisciplinary Research on Climate (MIROC6), Max Planck Institute Earth System Model (MPI-ESM1-2-LR), and Meteorological Research Institute Earth System Model (MRI-ESM2-0). We generate 50,000 TCs from the forcings of each of the 18 CMIP6 model-scenario pairs, for a total of 900,000 tracks. Due to climatological biases in the CMIP6 ensemble, we apply bias correction to the intensities of the synthetic TCs. Bias correction is implemented with a spatially-aware quantile delta mapping (Cannon et al., 2015) to align the distribution of historical TC intensities with historical observations, and preserve differences between corresponding quantiles in historical and future scenarios, as in Lipari et al. (2024) and Rice et al. (2025).

S2 Storm surge modeling

S2.1 ADCIRC simulations

The numerical model selected for generating the training dataset for DeepSurge is ADCIRC (Luettich Jr. & Westerink, 1991; Luettich et al., 1992; Pringle et al., 2021) v53.04. ADCIRC is an ocean circulation model that has been widely used in storm surge studies. The computational grid used in this study was based on an unstructured mesh developed by Dietrich et al. (2011)¹. It spans the U.S. East Coast, the Gulf of Mexico, and the Caribbean Sea, with the open boundary defined along the North Atlantic Ocean. The horizontal

¹Available at: <https://ccht.ccee.ncsu.edu/example-input-files-for-swanadcirc/>

resolution of the original mesh was relaxed to 15,467 nodes to balance computational costs and accuracy of the simulations, with a final resolution of approximately 25 km along coastlines and a 150 km resolution at the open boundary (Fig. S5a).

Historical tropical cyclone data for the North Atlantic was retrieved from NOAA’s International Best Track Archive for Climate Stewardship (IBTrACS) (Knapp et al., 2010, 2018). The North Atlantic IBTrACS dataset was subsampled to include only tracks contained within the extents of the ADCIRC model domain and a minimum storm length of 3 days, allowing for data gaps in wind speed and atmospheric pressure records of no more than six hours (gaps shorter than six hours were filled through linear interpolation). 279 tracks met these criteria (Fig. S5b). Wind fields were generated following the methodology outlined by Emanuel & Rotunno (2011) using each track’s maximum wind speed and radius of maximum wind, and a maximum radius of storm influence set at 300 km. Pressure fields were generated following the methodology presented by Holland (2008). No other forcings (e.g., tidal) were included in the ADCIRC simulations. To ensure the stability of the model, storm events shorter than 5 days were simulated using a ramp function to extend the total simulation time to 5 days (e.g., a 2-day ramp period for a 3-day storm event). Each simulation was executed with a 1-second time step and the resulting water levels (i.e., storm surge) were stored at 1-hour intervals over the entire computational domain.

S2.2 DeepSurge architecture & training

This section assumes some basic familiarity with neural network architectures. For an introduction to neural networks we recommend LeCun et al. (2015), and Emmert-Streib et al. (2020) for a more in-depth exploration.

The basic structure of the neural network, as detailed in Main Text Figure 1, has four stages: 1) encode the timeseries and spatial data separately, 2) convert them to compatible shapes and concatenate them together, 3) apply a Long Short-Term Memory (LSTM) (Hochreiter & Schmidhuber, 1997) layer to understand the temporal development, and 4) decode the features to predict a maximum surge level. To compactly notate tensor shapes, let T denote the (variable-length) time dimension, I denote the number of input features in the timeseries, and S denote the number of spatial images. The timeseries ($T \times I$) is encoded with a pair of one-dimensional convolutional layers with a kernel size of one, to expand the series to shape ($T \times 256$). The spatial stack ($64 \times 64 \times S$) is encoded with four successive 2-dimensional convolutional layers with striding and pooling to downsample to a vector (1×256) describing the spatial information. We then repeat this vector T times to create a tensor ($T \times 256$) that can be concatenated with the temporal features to create a $T \times 512$ tensor. This combined feature is passed through an LSTM layer—a recurrent sub-network that processes each step of a timeseries in the context of information remembered from all previous steps—which outputs a new sequence ($T \times 256$). Lastly, we decode these LSTM outputs with another series of 1-dimensional convolutional layers, resulting in a final output sequence ($T \times 1$). Taking the maximum over the T dimension returns the scalar maximum surge prediction for the storm at that given node. The network is constructed and trained in TensorFlow/Keras (Martín Abadi et al., 2015), and has a total of 1.7 million parameters.

Prior to training, 25% of storms in the dataset are set aside for testing, and never trained on. An additional 15% of remaining storms are used as the validation set, to test for overfitting during the training process. Since extreme surge levels are of more interest and simultaneously more rare in the training data, two adjustments are made: Each example’s loss is weighted proportional to the ADCIRC peak surge height in meters plus one (e.g., a surge of 6 m has a weight of 7, while a surge of 0 m has a weight of 1), and examples with ADCIRC peak surges below 1 meter are sampled less frequently to correct for their over-representation in the dataset. Training occurs in epochs, each consisting of 500 batches with a batch size of 32. During training, low levels of zero-centered Gaussian noise ($\sigma = 1e-3$) are added to the inputs as a simple regularization mechanism. We use the Adam optimizer (Kingma & Ba, 2014), and the mean-squared error between the maximum neural network prediction and maximum ADCIRC modeled surge as the loss target. At the end of each epoch, the loss on the validation set is assessed, and the best model iteration according to this metric is saved. The learning rate begins at $2e-3$, and is multiplied by a factor of 0.2 after any three consecutive epochs with no validation loss improvement. Training is stopped after six consecutive epochs with no validation loss improvement. This architecture was developed and tuned over numerous manual iterations, including experimenting with learning rates, batch sizes, alternate model structures, batch normalization, dropout, scaling the width and depth of the network, different recurrent

units, and regularization techniques.

S2.3 DeepSurge computational efficiency

For an approximate comparison of the computational speedup provided by our method, we predict Hurricane Katrina’s storm surge using both DeepSurge and ADCIRC on high-performance computing systems. We find DeepSurge to be approximately 12.5x faster in terms of CPU-hours, with an upper bound of 96x when predicting hundreds of storms in sequence (since DeepSurge’s initialization stage is the bulk of the computational burden, which can subsequently be shared across multiple simulations). Even with this significant speedup, the computational expense of simulating 900,000 storms is not insignificant; approximately 350 high-performance compute node-hours were utilized (with 256 cores per node, $\sim 90,000$ core-hours).

S2.4 DeepSurge validation & sensitivity analysis

DeepSurge demonstrates promising generalization skill on the test set, which consists of 71 storms that the model has never been trained or tuned on. When compared to the corresponding ADCIRC simulations, DeepSurge achieves an 81.5% R^2 score, a mean squared error of 0.224 m, and a mean absolute error of 0.258 m in predicting peak surge heights per node. As error metrics in terms of raw surge height are difficult to contextualize on their own, we later assess the sensitivity of our inundation results to the model’s biases and errors.

To compare with observed storm surge data, we perform a validation against NOAA tide gauge observations². All available peak tide gauge measurements within a 300 km radius of each test-set storm’s track are collected and co-located with the predictions from the nearest ADCIRC/DeepSurge node. Peak surge for each tide gauge is calculated as the maximum difference between observed water level and expected tide. Only verified data with gaps of less than one hour during the lifetime of the storm are considered, resulting 194 valid gauge observations. Although this is highly accurate data, it is notably incomplete; tide gauges often fail or malfunction during extreme surge events, with failure observed at surge heights as low as 1.22 m (see Needham (2014)’s Figure 5.1). This effect causes a fairly strong sampling bias toward smaller surge levels, with the largest observed surge in this collection being 3.1 m despite the fact that a number of storms in the sample (including 2005’s Hurricane Katrina) are known to have generated much larger surges. Gauge observations may be influenced by factors not modeled by ADCIRC or the neural network, such as rainfall, river discharge, and background non-cyclonic winds, which makes them an imperfect comparison for our surge-only ADCIRC and DeepSurge simulations, though we expect these influences to be small relative to TC-driven surge in most cases. DeepSurge shows reasonable skill in capturing these gauge-observed surge peaks, with error metrics ($R^2 = 0.403$, MAE = 0.474m, RMSE = 0.664m) similar to the ADCIRC simulations ($R^2 = 0.427$, MAE = 0.543m, RMSE = 0.882m). Pearson and Spearman correlations are highly significant ($p \ll 0.001$). Possibly due to the negative sampling bias of the gauge observations, both DeepSurge and ADCIRC exhibit positive mean biases (+0.217m and +0.203m respectively).

Additionally, a sensitivity analysis is performed to understand how the biases of the DeepSurge model may impact our final inundation estimates. Specifically, we estimate the bias at each DeepSurge node as the mean of the biases at all gauge observations within three degrees of the node, weighted inversely by distance. This process is averaged over 200 bootstrap samples of the gauge bias observations for robustness. The derived bias (Fig. S6) is generally positive as noted prior, with near zero bias (< 0.25 m) in the western Gulf of Mexico and eastern Florida, moderate bias (generally < 0.5 m) in the rest of the Gulf and Southeast, and larger biases in the Northeast—though the sample size in that region is notably less robust, with 20 total gauge-prediction pairs north of $37^\circ N$ caused by only 4 storms. Correcting for this estimated bias in DeepSurge’s 100-year surge event and recalculating inundation risk results in an 18% reduction in historical-period population affected, and a 14% reduction in future-period population affected. Use of these bias-corrected totals actually indicates an even stronger relative change in inundation risk in the future of +57%, compared with the +50% found using the uncorrected totals. At the individual state level, all states in the Gulf and Southeast see corrections of under $\pm 30\%$ (and all but Georgia and South Carolina under $\pm 20\%$), with the near-zero biases in Texas. Corrections are much larger in the Northeast, exceeding -50% in Massachusetts and New Jersey, though again we note the much lower confidence in estimated biases there.

²Accessible from the Tides & Currents API: <https://api.tidesandcurrents.noaa.gov/mdapi/prod/#>

Given the limited sample size, incompleteness of the tide gauge records, and confounding factors previously discussed, we treat these results as only rough indications of the directions and magnitudes of DeepSurge biases. For these reasons, and because the uncorrected total actually present a more conservative view of relative future changes in risk, we choose to report the uncorrected totals in the main manuscript.

S2.5 Validation of modeled 100-year surge height

To quantitatively verify that the combination of DeepSurge and RAFT are producing accurate 100-year surge heights, we compare our ensemble median return levels with the historical 100-year event observational estimates from Needham (2014), who undertook an exhaustive analysis of the historical storm surge record 1900–2014 throughout the Gulf of Mexico, and three of independent surge modeling techniques: Gori et al. (2022) forced a similar synthetic TC model with NCEP reanalysis for a historical period (1980–2005) and eight CMIP6 GCMs for a future period (2070–2100 under SSP5-8.5) to model the 100-year storm *tide* above mean higher high water (MHHW) with a peaks-over-threshold approach using ADCIRC. Muis et al. (2023) forced the Global Tide and Surge Model (a hydrodynamic model based on Delft3D) with historical ERA5 reanalysis (1985–2014) as well as five high-resolution CMIP6 models for a historical (1950–2014) and near future (2015–2050 under SSP5-8.5) period, using a peaks-over-threshold approach to estimate 100-year storm surge levels. Lastly, for a comparison with a simple parametric model we generate surges with the Storm Surge Hazard Potential Index (SSHPI) developed by Islam et al. (2021), forced by the same RAFT synthetic TCs as DeepSurge. The historical 100-year estimates from each of the modeling methods are presented in Fig. S9.

The 100-year estimates from Needham (2014)³, Gori et al. (2022)⁴, and Muis et al. (2023)⁵ are all directly published with no additional computation performed on our part, while Storm Surge Hazard Potential Index (SSHPI) (Islam et al., 2021) estimates were derived using the following method: Predictions were computed by applying the SSHPI equations (see Islam et al. (2021), their equations 4 and 5) to the same 900,000 synthetic TCs used to force DeepSurge. SSHPI-derived surge is computed at hourly timesteps for all nodes within 0.5 degrees of the storm center, and the maximum predicted surge at each node is saved. Because the SSHPI formulation requires a measure of the mean radius of 50-knot winds (R_{50kt} , in nautical miles) which is not directly modeled in our synthetic TCs, a linear regression on maximum wind speed (V_{max} , in knots), latitude (degrees North), and radius of maximum wind (R_{mw} , in nautical miles) was derived from all available observations ($n = 222$) in the HURDAT database (Jarvinen et al., 1984). This simple formulation achieves a Pearson’s correlation of 0.83 and R^2 of 0.68:

$$R_{50kt} = 0.596 \cdot V_{max} + 0.853 \cdot R_{mw} + 2.074 \cdot \text{lat} - 69.044$$

The three methods’ predictions are all co-located to the nearest node within 0.15 degrees, which enables consistent comparison between methods at 651 locations along the U.S. coast.

The analysis by Needham (2014) reveals 100-year surge levels ranging from 2.53 m (Cedar Key, Florida) to 7.95 m (Bay St. Louis, Mississippi). Naturally these observations are subject to a great deal of random variability, as the chance occurrence or non-occurrence of particular extreme events (e.g., Hurricane Katrina) within this particular 115-year sample will bias the estimates; still, they remain the best available approximation of the spread of 100-year surge levels in this region. Co-locating the Needham (2014) estimates with the other methods ($n = 18$) reveals that DeepSurge achieves the most comparable cumulative distribution of 100-year surge magnitudes (Fig. S7). However, all methods including DeepSurge have insignificant ($p > 0.05$) Spearman correlations against the spatial pattern of the sparse Needham estimates.

In addition to comparing against the historical records, each of these methods’ 100-year return level estimates are cross-compared. Given the wide variability in magnitudes, Spearman’s rank correlation is used as a scale-invariant measure of pattern similarity. As shown in Figure S9, DeepSurge has the best Spearman correlation with every other method, for both the historical and future periods (excepting the high correlation between the Muis et al. (2023) variants). The larger sample of synthetic TCs utilized in our method may allow it to capture a more robust signal and be less subject to random noise, which enables stronger agreement with the three alternatives than they exhibit between themselves.

³Data available in Needham (2014)’s Table 5.9

⁴Data available at: <https://doi.org/10.17603/ds2-gv07-kf03>

⁵Data available at: <https://doi.org/10.24381/cds.6edf04e0>

S3 Inundation modeling

S3.1 CA-Surge algorithm

CA-Surge is a simple “bathtub-style” inundation model, with frictional attenuation. Conceptually, the algorithm starts with a water surface elevation (surge height) in the open ocean, and fills inland pixel-by-pixel until the water is not able to flow any further. The water depth for a pixel is computed as the difference between the water surface elevation and the ground elevation, with the water surface elevation being lowered (attenuated) as it moves across a pixel, in accordance with its land cover class.

The algorithm uses 3 input rasters and an attenuation multiplier parameter. All three rasters must be the same size and aligned with each other. DEM-Raster contains a digital elevation model of the study domain. Each cell (pixel) gives the height above (or below) mean sea level (in meters). Surge-Raster contains a surge height (in meters) above mean sea level for all cells (pixels) where surge originates (usually over the open ocean near the coast). All other cells (pixels) contain 0. Attenuation-Raster contains the surge attenuation values. Each cell (pixel) contains the drop in surge (in meters) as water horizontally traverses the cell. For example, if the cell contains the value 0.01, it means that the surge will be reduced by 1 centimeter if the surge traverses the cell. Attenuation-Multiplier is a numerical value between 0 and 1 that is applied to the values in the Attenuation-Raster, in accordance with (Vafeidis et al., 2019). If the multiplier is 0, then no attenuation will be applied to the surge as it traverses the raster cells (pixels). If the multiplier is 1, then the full attenuation value will be subtracted from the surge as it traverses the raster cells. CA-Surge is then defined by the following algorithm:

Algorithm 1 CA-Surge

Four internal matrices that match the size of the input rasters are initialized:

- *el*: contains the DEM-Raster data.
- *att*: contains the Attenuation-Raster data.
- *wse*: contains the water surface elevation. The cells are initialized to the values of the Surge-Raster.
- *h*: contains the height of the surge water above the DEM elevations. Each cell is initialized to *wse* minus *el*. The cell is set to 0 if any of the following conditions is true for the cell: the *wse* cell contains no data, the *el* cell contains no data, or *wse* minus *el* is less than or equal to 0. Cells that are set to a positive, non-zero value are added to a list of cells to a check list.

The model then iterates through the following steps:

1. If the check list is empty, processing is complete, and the *h* matrix is output as a raster.
 2. For each cell in the check list (the “current cell”), apply the following to each of the current cell’s eight adjacent neighbors (the “neighbor cell”):
 - (a) Compute $waterSurface = wse - (att * distance * Attenuation-Multiplier)$, where *wse* and *att* are from the current cell, and distance is 1.0 for vertical and horizontal neighbors and $\sqrt{2}$ for diagonal neighbors.
 - (b) Compute $depth = waterSurface - el$, where *el* is from the neighbor cell.
 - (c) If *depth* is greater than 0 and *el* is not empty and the neighbor cell has not already been processed, or *depth* is greater than the *h* of the neighbor cell:
 - *wse* of the neighbor cell is set to *waterSurface*
 - *h* of the neighbor cell is set to *depth*.
 - The neighbor cell is added to the check list of the next iteration.
-

S3.2 Validation of inundation modeling

Accurate observations of inundated area from historical storm surge events are generally difficult to come by. Some of the best available data to our knowledge are FEMA high-water marks (HWMs) surveyed following 2005’s Hurricane Katrina by contractor URS Group (Group, 2006a,c,b). This data contains a larger sample of surveyed points than most other HWM surveys, provides HWM elevation, and crucially labels each mark as caused to wave action, riverine flooding, or sustained storm surge, which is not common in other surveys. This enables an accurate evaluation of the surge-only DeepSurge method without complications from wave run-up and riverine flooding. Although the most famous flooding from this event was in Louisiana, much of it was due to or compounded by failures in the levee system; since these factors are outside of the modeling abilities of DeepSurge and CA-Surge, we focus on Mississippi and Alabama in this comparison, which received substantial flooding as well. We estimate inundation from this data by linearly interpolating a 3d water level surface from all HWMs, subtracting USGS ground elevation (Danielson & Gesch, 2011) to determine height-above-ground, and filtering all pixels which are not hydrologically connected to the ocean (Fig. S10a). Ground elevation is computed as the midpoint between the median and minimum elevation in each pixel to account for water’s tendency to take the lowest available path. The extent of flooding seems to be roughly bounded by the outer extent of high-water mark locations in Fig. S10a which suggests this method is capturing the underlying hydrodynamics that caused the marks. LandScan data from all inundation pixels is used to estimate inundated populations, which are then aggregated to census-tracts (Fig. S10b). DeepSurge and CA-Surge applied to the best track of Katrina (Fig. S10c) reasonably captures the pattern of the HWM-derived results in terms of percentage of population affected at the tract level (Pearson $r = 0.77$, Spearman $r = 0.78$, p -values $\ll 0.001$, $R^2 = 0.59$, MAE = 9.1 percentage points).

To validate the combination DeepSurge and CA-Surge for the entire coastline, we compare our state-level estimates of historical population at risk from 100-year storm surge inundation with those from Crowell et al. (2010) (see their Table 1), who estimate the 100-year coastal flood risk from the extremely high-resolution Flood Insurance Rate Maps (FIRMs) produced by FEMA. These FIRMs are developed with detailed and manual process combining modeling, observations, expert survey, and community input. Because of the effort required, FIRMs in some areas may be decades old. Additionally, since the maps do not differentiate between causes of flooding, Crowell et al. (2010) manually estimate the separation of surge- and riverine-driven flooding to isolate the former. Lastly, these coastal 100-year flood zones are spatially joined with census block-group population estimates from the 2000 census. Notably, they assume that population density is distributed uniformly within block-groups. While these approximations are possible sources of error, this FIRM-based assessment still represents one of the best available estimates of 100-year surge risk for the whole US coastline. We find that our historical-period 100-year inundation estimate correlates very highly with Crowell et al.’s totals, with Pearson and Spearman correlations of 0.95 and 0.87 respectively ($p \ll 0.01$). Interestingly, our DeepSurge & CA-Surge method shows a negative bias in population affected for most states (Fig. S11)—most significantly for barely-affected states e.g. Pennsylvania—which runs counter to the positive biases found against tide gauge observations and high-water mark analysis in previous sections. These differences are perhaps due to the inclusion of wave action effects in the FEMA modeling, or inaccuracies in either (or both) of DeepSurge or Crowell’s methodologies.

S4 Drivers of change

It is difficult to assess the contributions of individual storm characteristics to DeepSurge-predicted surge heights due to the black-box nature of neural networks and the complex, nonlinear, and time-dependent nature of the underlying physics. However, simple parametric models such as SSHPI (Islam et al., 2021, 2022) enable the evaluation of the approximate direction and magnitude of effect that each storm characteristic has on surge height. SSHPI predicts peak surge based on the multiplicative combination of four factors: storm intensity (maximum wind speed), storm size (radius of 50-kt winds), storm translation speed, and bathymetry (distance to 30 meter isobath). As Figure S12a-b shows, SSHPI projects a much more homogeneous increase in surge risk across the US coastline than DeepSurge, though the two do broadly agree on the sign of the change south of 35°N , while agreement is more mixed in the Northeast. Disagreements may be largely explained by SSHPI’s indifference to the direction of storm motion; in regions where storms tend to make landfall at indirect angles relative to the coastline (e.g. much of the Northeast, Fig. S2a) or

are projected to increasingly do so in the future climate (e.g. western Florida, S2b), SSHPI's formulation is less reliable. Nevertheless, since it is forced with the same set of TCs as DeepSurge, disassembling SSHPI into its components is instructive: Increasing storm intensities are a strongly positive contribution to surge height across the domain (Fig. S12c), while slightly larger radii of 50-kt winds—due largely to increasing intensities—are further weakly positive (Fig. S12d). Decreasing storm translation speeds in the future period result in lower surges on open coastlines, and slightly larger surges in bays and estuaries (Fig. S12e). In total, increasing storm intensity dominates the trend across nearly the entire coastline (Fig. S12f).

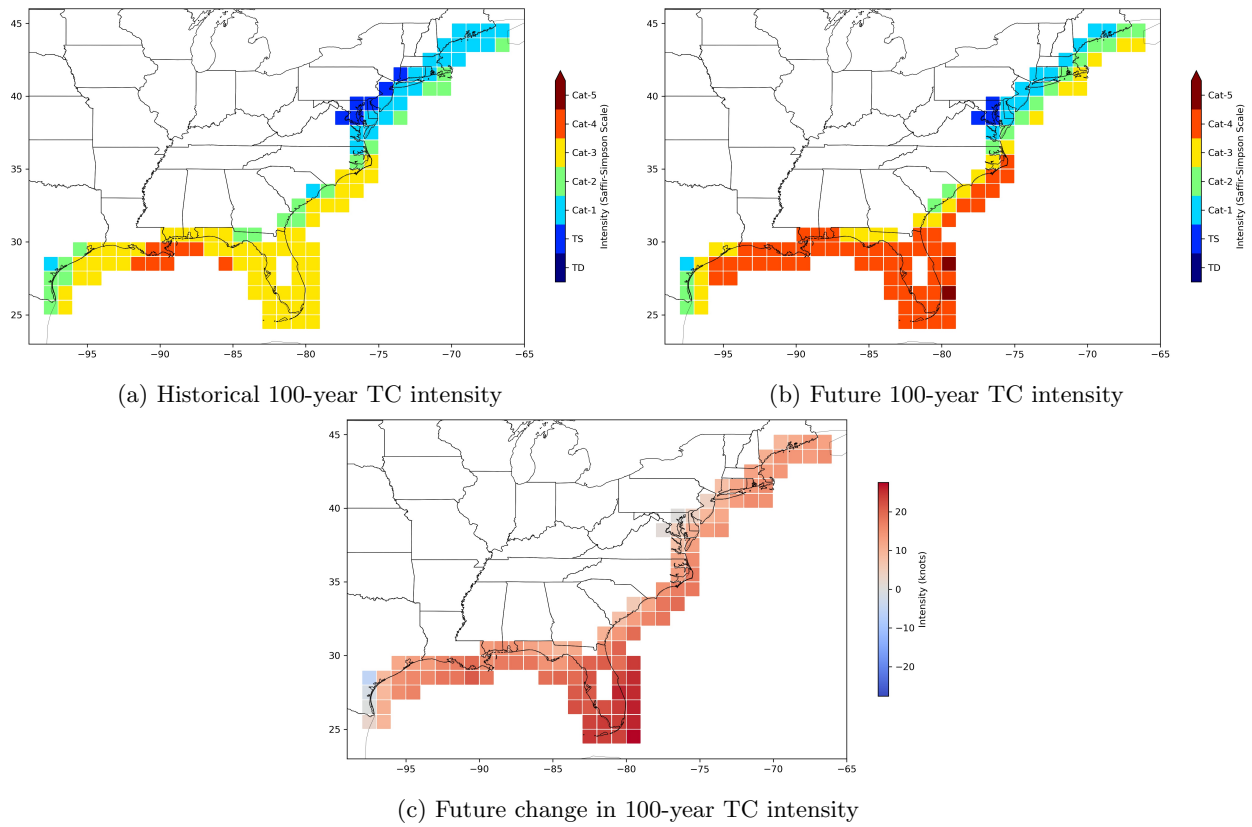


Figure S1: Ensemble mean 100-year synthetic TC intensity for the (a) historical and (b) future periods, and (c) their difference.

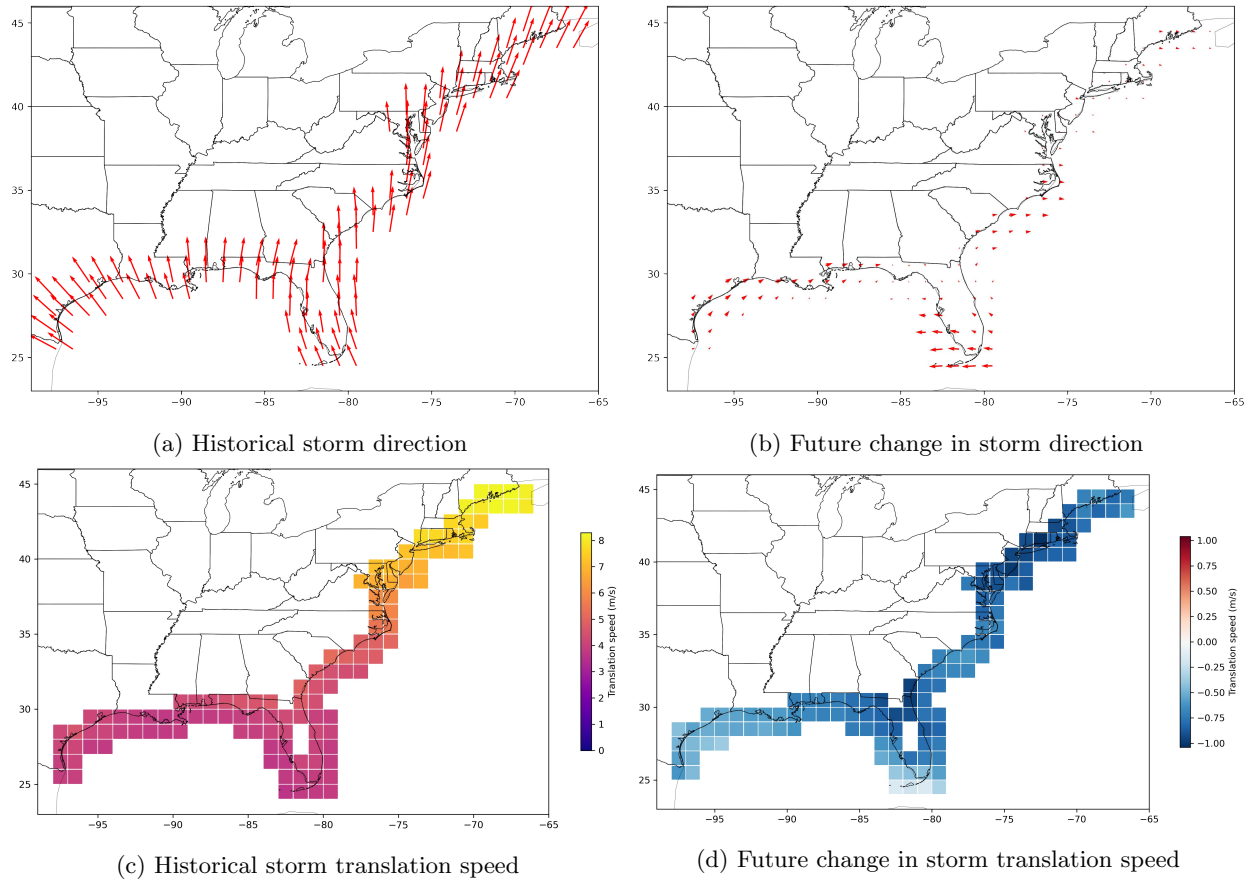
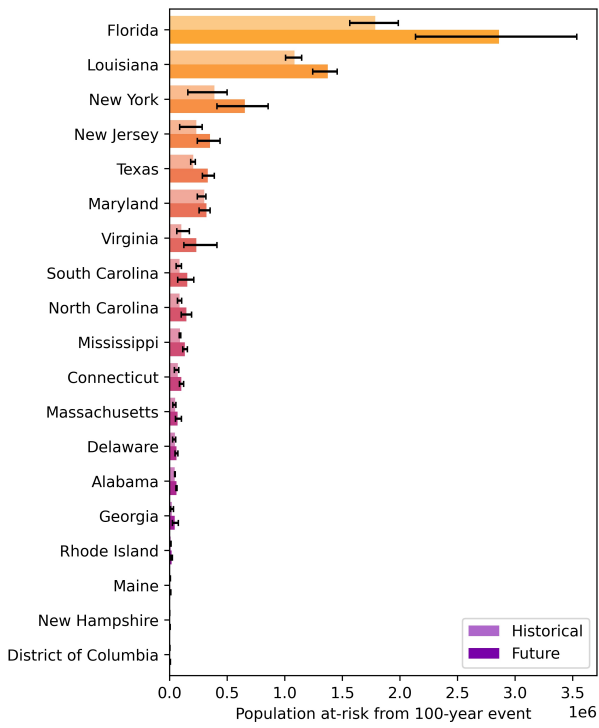
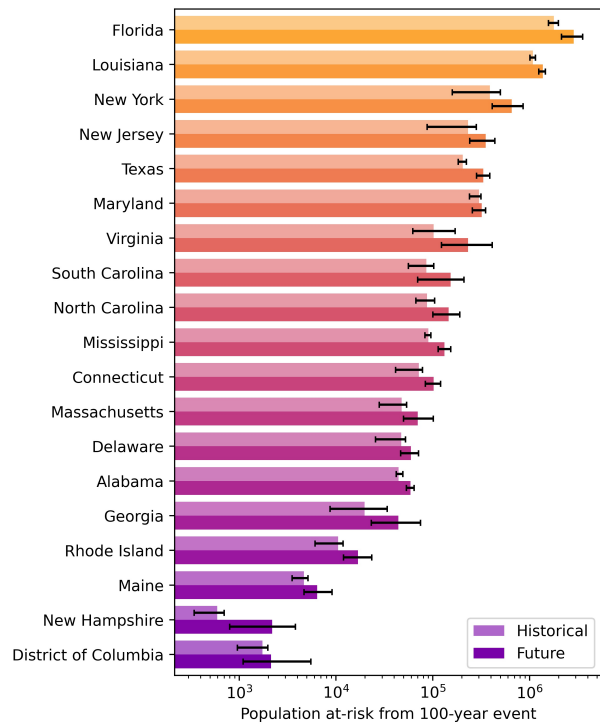


Figure S2: **(a-b)** Average movement direction for all synthetic TCs (of at least Category 1 Saffir-Simpson strength) in the historical period weighted by magnitude of storm translation speed, and the future change. Arrows in panel **b** are 2x scaled relative to **a** for clarity. **(c-d)** Average synthetic TC movement speed in the historical period weighted by storm intensity, and the future change.



(a) Linear scaling



(b) Log scaling

Figure S3: Median estimate of population at risk from 100-year flood event in the historical and future periods for each state, along with 90% uncertainty intervals, (a) linearly scaled, and (b) logarithmically scaled for clarity in less-affected states.

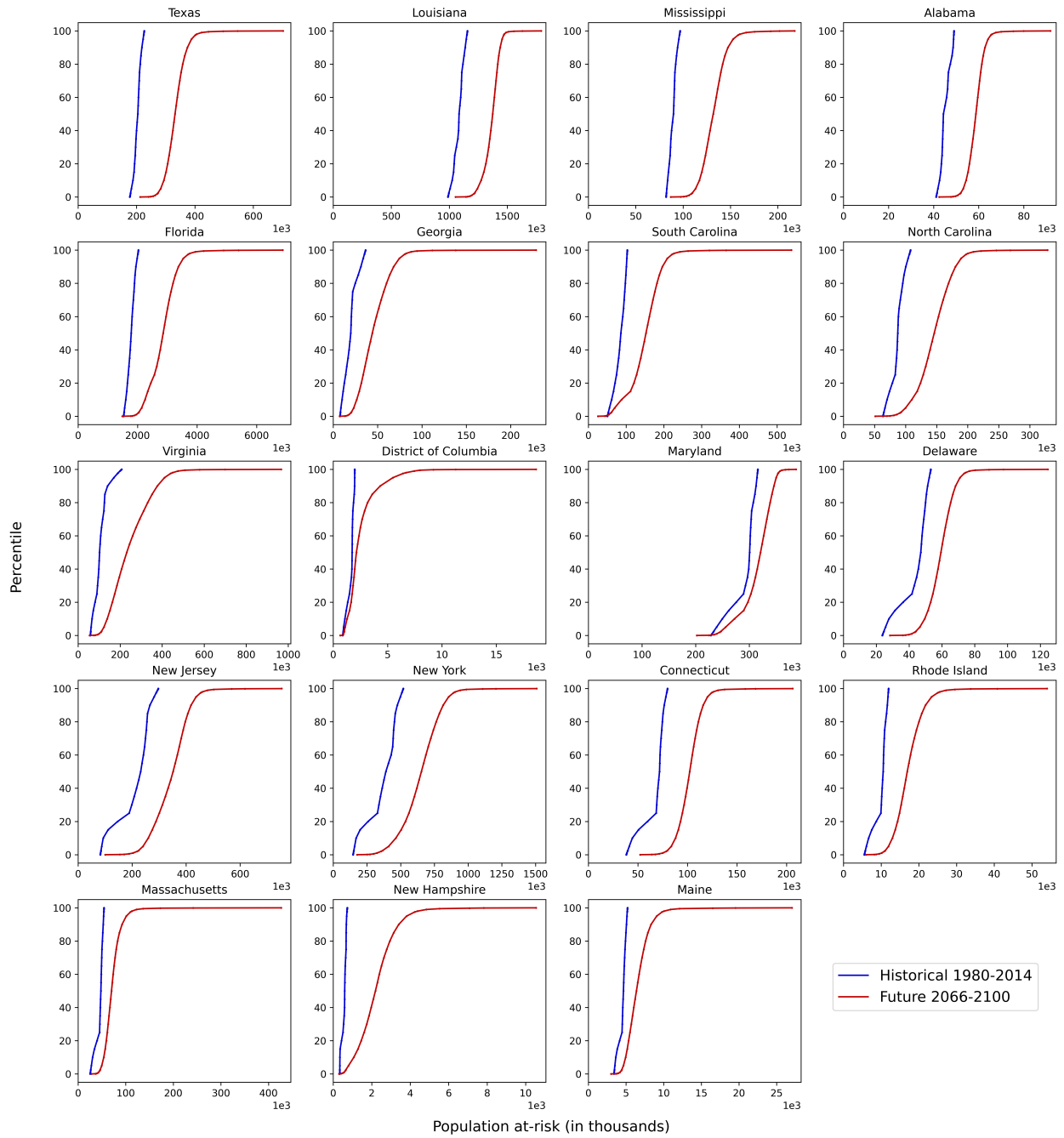


Figure S4: Empirical cumulative distribution functions (eCDFs) of population at risk from DeepSurge-modeled 100-year storm surge flooding for each state.

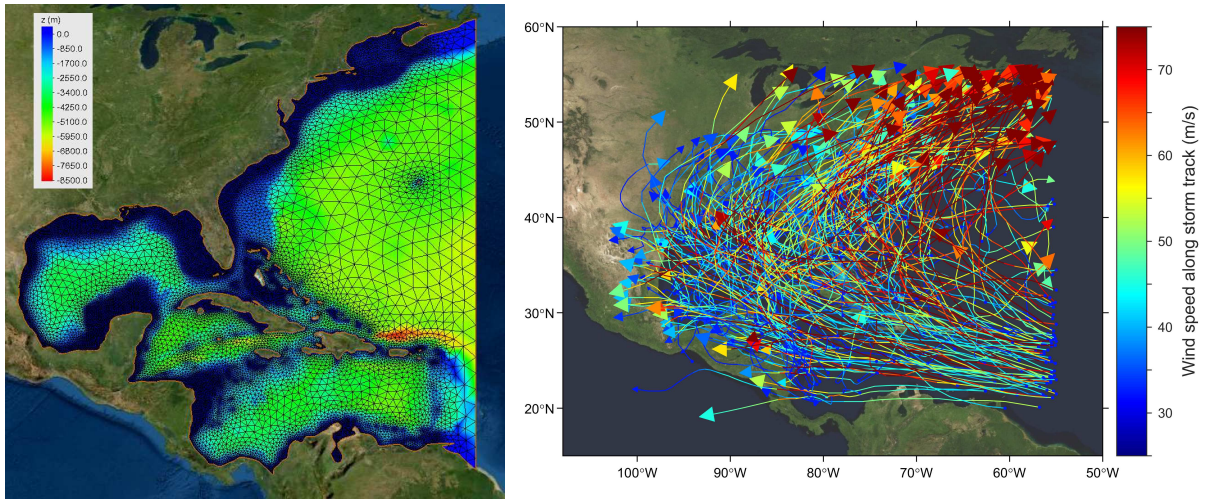


Figure S5: (a) ADCIRC domain, triangular elements of unstructured grid, and bathymetry colormap. (b) Historical TC tracks simulated by ADCIRC used for training.

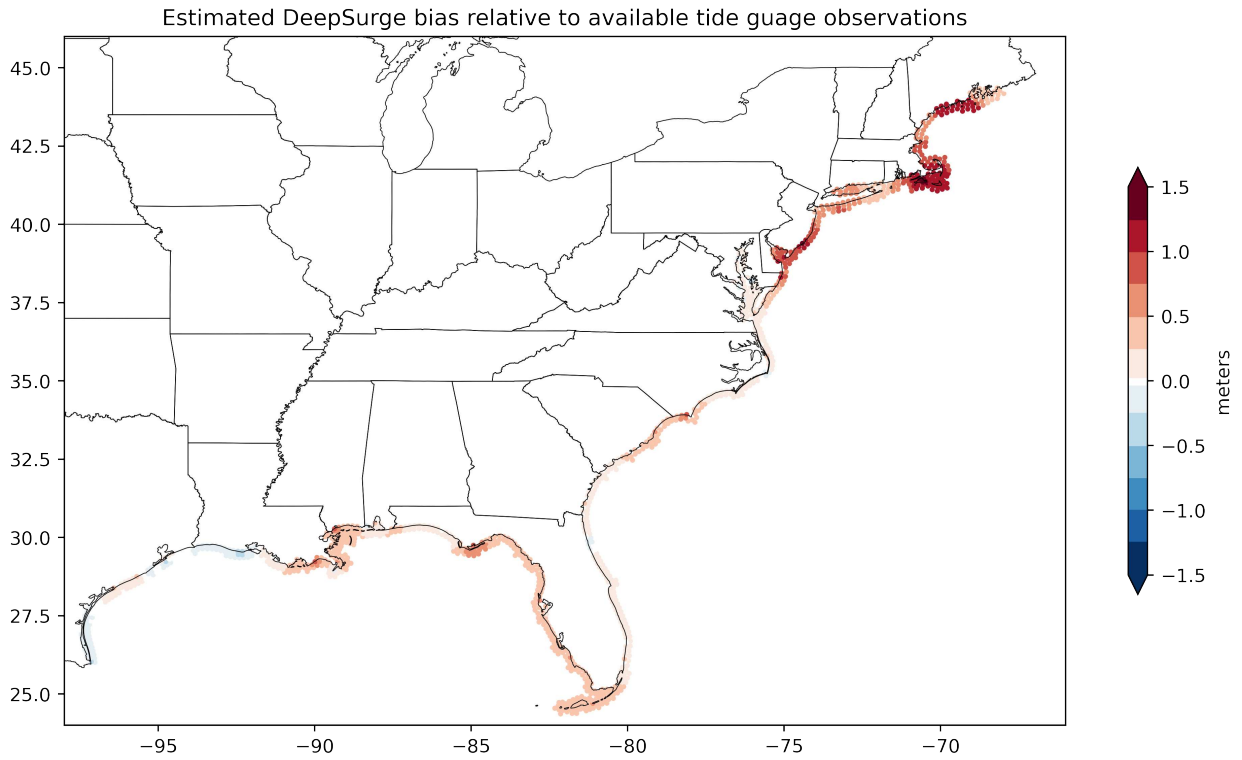


Figure S6: Estimated spatial mean bias of DeepSurge relative to tide gauge observations. Note that small sample sizes make the error estimates in the Northeast much less robust.

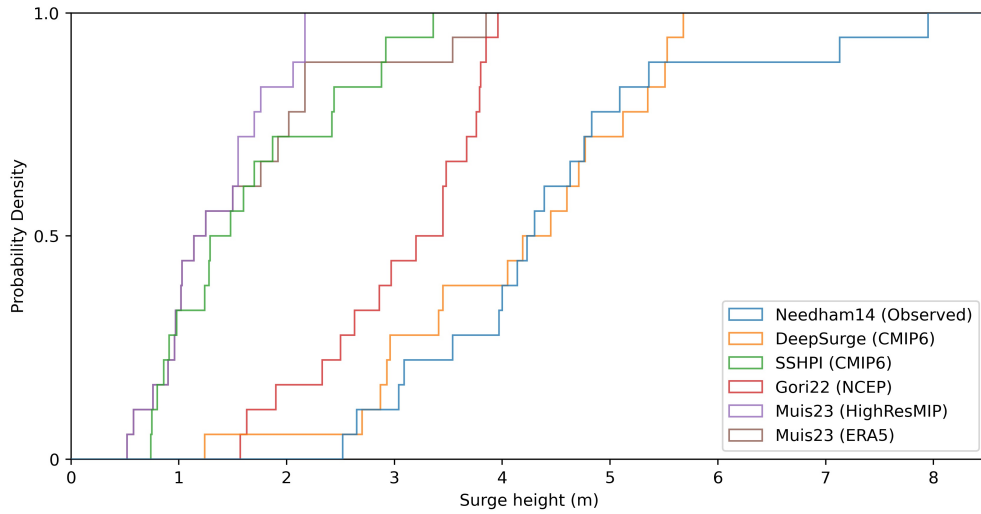


Figure S7: Empirical cumulative distribution functions (eCDFs) of historical 100-year surge heights from 18 locations across the Gulf Coast estimated by the Needham (2014) compared to each modeling method. The methods are: DeepSurge (ours), Gori et al. (2022), Muis et al. (2023), and SSHPI (Islam et al., 2021), with the climate data used to force the model listed in parentheses.

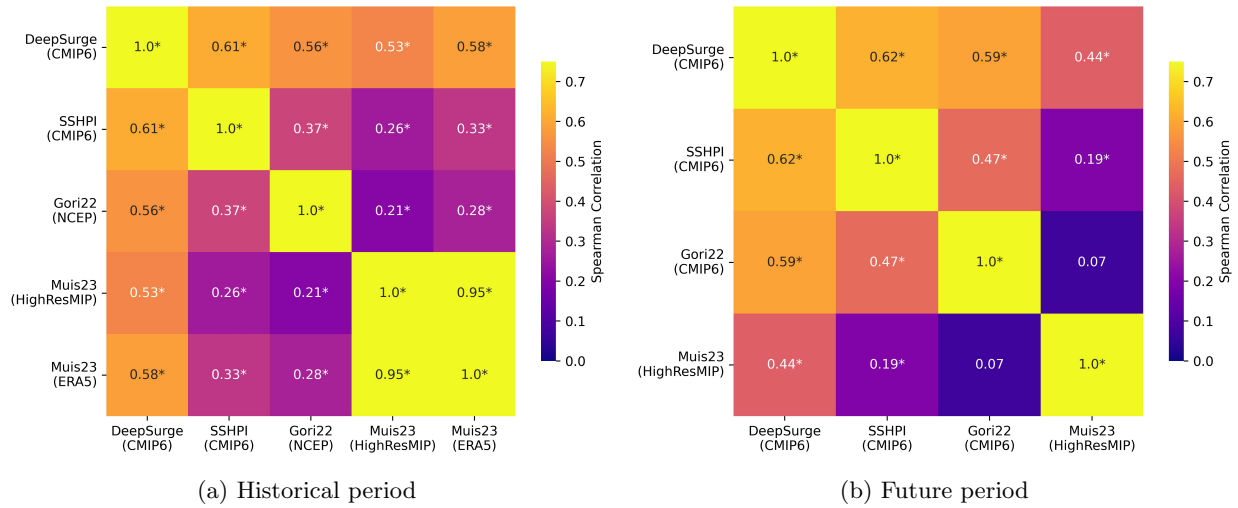


Figure S8: Spearman correlations between methods for the spatial distribution of the 100-year return level, as estimated in each method's respective (a) historical and (b) future period. Asterisks indicate significance at the 95% level. Note that these methods have varying definitions of the historical and future time period. The methods are: DeepSurge (ours), Gori et al. (2022), Muis et al. (2023), and SSHPI (Islam et al., 2021), with the climate data used to force the model listed in parentheses.

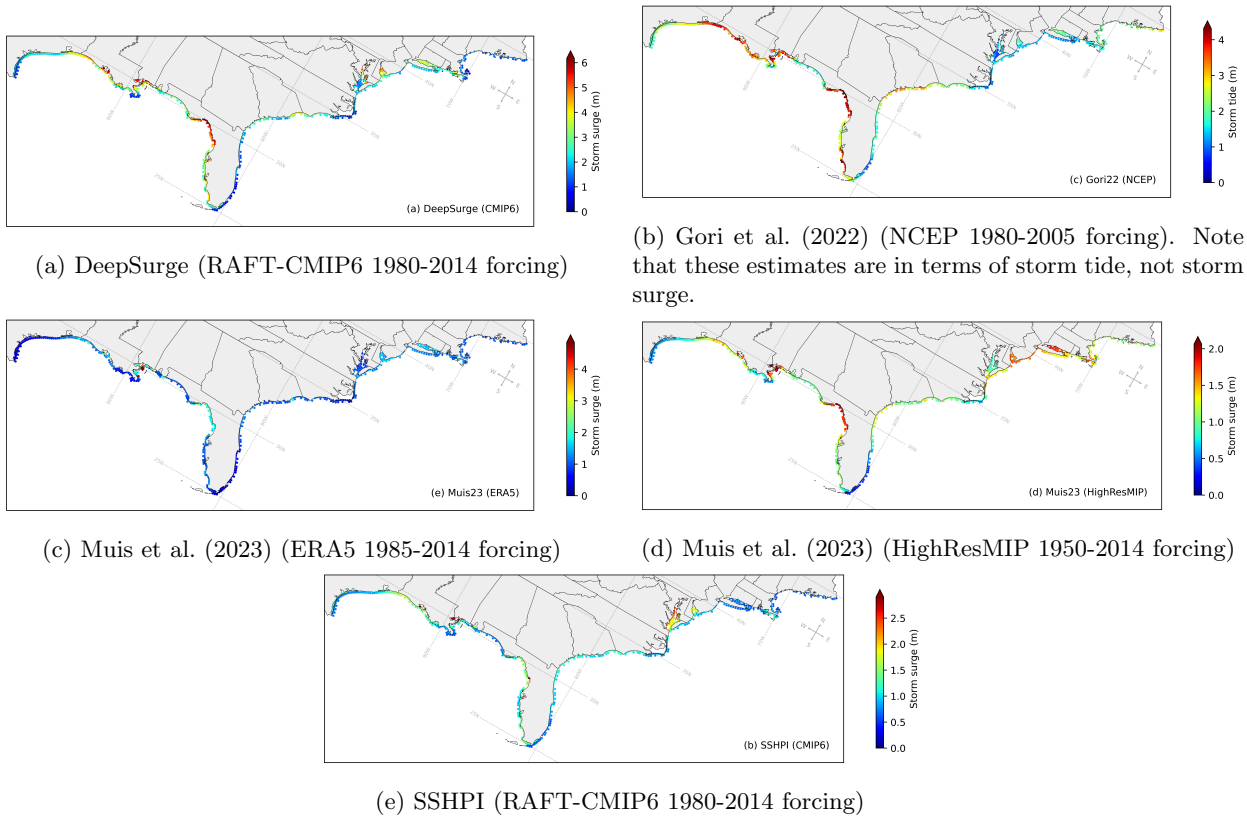
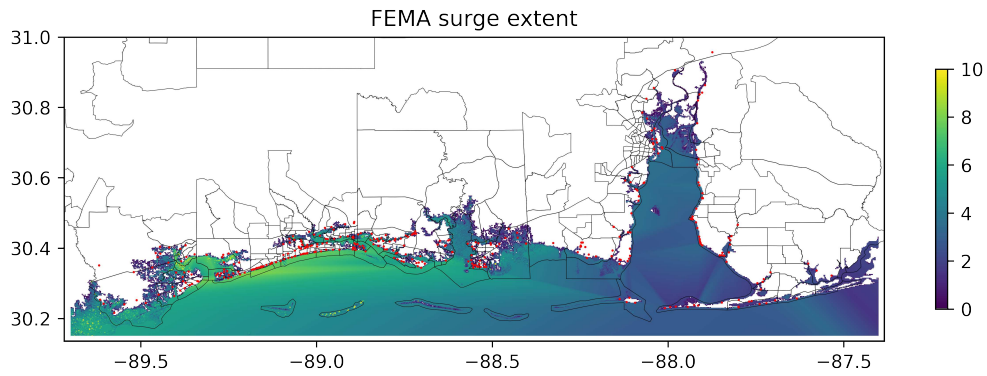
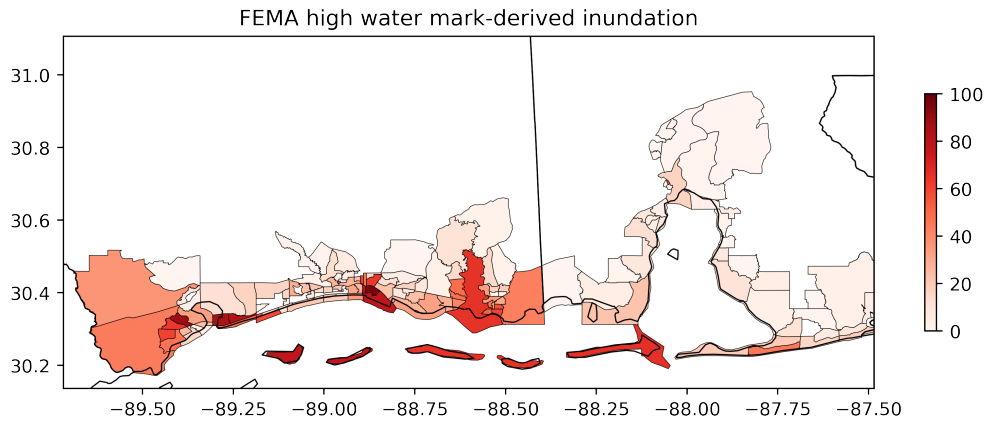


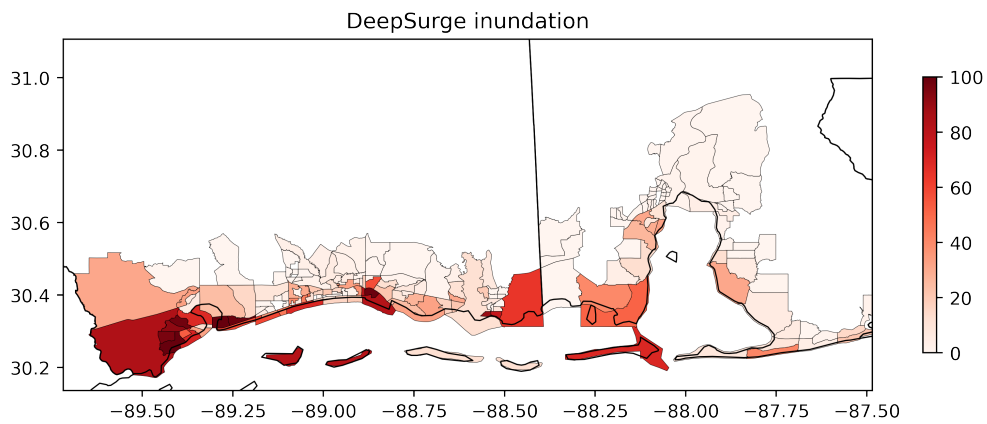
Figure S9: The 100-year surge level estimates from five modeling methods, for their respective historical periods. Note that the vastly varying magnitudes necessitate different colorscales, with the colorscale maximum set to the 99th percentile of the data for each.



(a) Inundation surface estimated from FEMA high-water marks. Red dots indicate location of high water marks.



(b) Population affected estimated from FEMA high-water marks



(c) Population affected estimated by DeepSurge and CA-Surge

Figure S10: Inundated (a) area and (b) population at the census-tract level estimated from FEMA high-water marks from Hurricane Katrina (2005), in Mississippi (left half) and Alabama (right half). (c) Inundated population estimated by our method. Note that since census tracts have roughly the same number of residents, large tracts are not any more important than small tracts. Some islands are part of mainland census tracts.

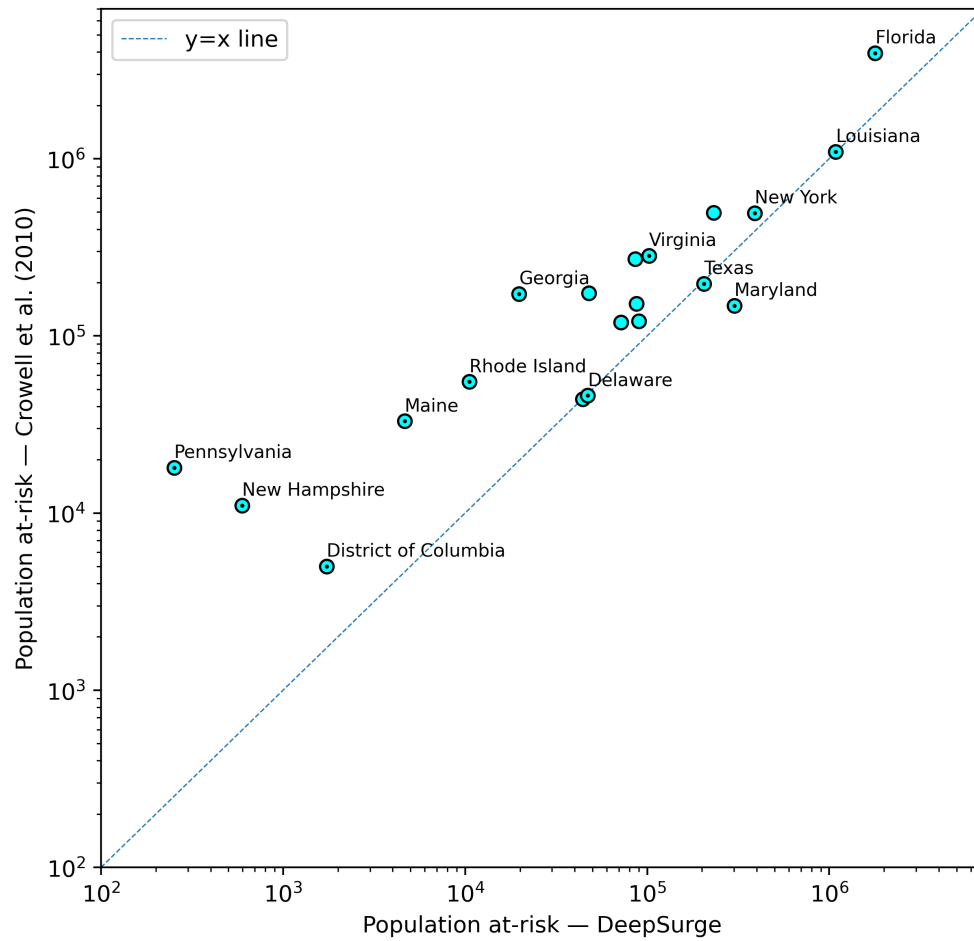


Figure S11: Comparison between historical 100-year inundation estimates from Crowell et al. (2010) and our method. They exhibit Pearson and Spearman correlations of 0.95 and 0.87 respectively ($p \ll 0.01$).

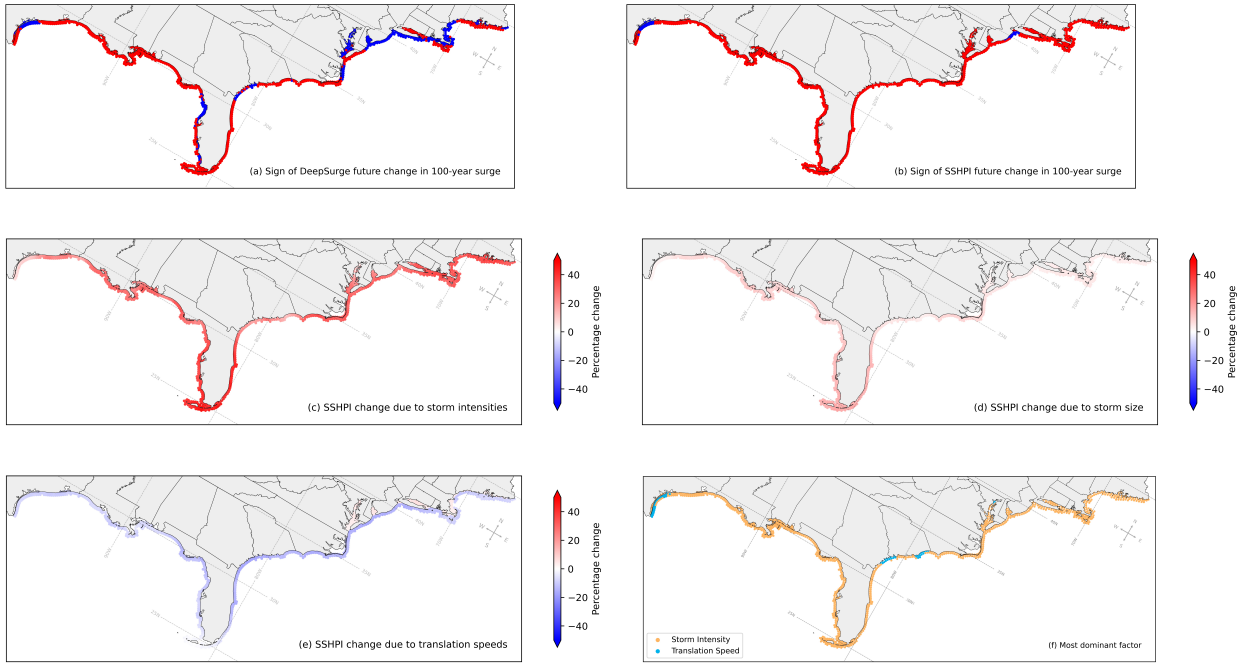


Figure S12: Sign of future change in 100-year surge height, as projected by **(a)** DeepSurge, and **(b)** SSHPI (red is positive, blue is negative). Percentage change in the future-climate SSHPI-derived surge for all events with return periods of ≥ 100 years, due to **(c)** storm intensity **(d)** storm size and **(e)** storm translation speed. **(f)** The largest contributing factor at each node.

References

- Balaguru, K., Xu, W., Chang, C.-C., Leung, L. R., Judi, D. R., Hagos, S. M., Wehner, M. F., Kossin, J. P., and Ting, M. Increased U.S. coastal hurricane risk under climate change. *Science Advances*, 9(14):eadf0259, April 2023. doi: 10.1126/sciadv.adf0259. URL <https://www.science.org/doi/full/10.1126/sciadv.adf0259>. Publisher: American Association for the Advancement of Science.
- Cannon, A. J., Sobie, S. R., and Murdock, T. Q. Bias Correction of GCM Precipitation by Quantile Mapping: How Well Do Methods Preserve Changes in Quantiles and Extremes? *Journal of Climate*, 28(17):6938–6959, September 2015. ISSN 0894-8755, 1520-0442. doi: 10.1175/JCLI-D-14-00754.1. URL <https://journals.ametsoc.org/view/journals/clim/28/17/jcli-d-14-00754.1.xml>. Publisher: American Meteorological Society Section: Journal of Climate.
- Chavas, D. R., Camargo, S. J., and Tippett, M. K. Tropical cyclone genesis potential using a ventilated potential intensity, April 2024. URL <http://arxiv.org/abs/2404.01572>. arXiv:2404.01572 [physics] version: 1.
- Crowell, M., Coulton, K., Johnson, C., Westcott, J., Bellomo, D., Edelman, S., and Hirsch, E. An Estimate of the U.S. Population Living in 100-Year Coastal Flood Hazard Areas. *Journal of Coastal Research*, 262:201–211, March 2010. ISSN 0749-0208, 1551-5036. doi: 10.2112/JCOASTRES-D-09-00076.1. URL <http://www.bioone.org/doi/abs/10.2112/JCOASTRES-D-09-00076.1>.
- Danielson, J. J. and Gesch, D. B. Global multi-resolution terrain elevation data 2010 (GMTED2010). USGS Numbered Series 2011-1073, U.S. Geological Survey, 2011. URL <http://pubs.er.usgs.gov/publication/ofr20111073>. Code Number: 2011-1073 Code: Global multi-resolution terrain elevation data 2010 (GMTED2010) Publication Title: Global multi-resolution terrain elevation data 2010 (GMTED2010) Reporter: Global multi-resolution terrain elevation data 2010 (GMTED2010) Series: Open-File Report.
- Dietrich, J. C., Westerink, J. J., Kennedy, A. B., Smith, J. M., Jensen, R. E., Zijlema, M., Holthuijsen, L. H., Dawson, C., Luettich, R. A., Powell, M. D., Cardone, V. J., Cox, A. T., Stone, G. W., Pourtaheri, H., Hope, M. E., Tanaka, S., Westerink, L. G., Westerink, H. J., and Cobell, Z. Hurricane Gustav (2008) Waves and Storm Surge: Hindcast, Synoptic Analysis, and Validation in Southern Louisiana. *Monthly Weather Review*, 139(8):2488–2522, August 2011. ISSN 1520-0493, 0027-0644. doi: 10.1175/2011MWR3611.1.
- Emanuel, K. and Rotunno, R. Self-Stratification of Tropical Cyclone Outflow. Part I: Implications for Storm Structure. *Journal of the Atmospheric Sciences*, 68(10):2236–2249, October 2011. ISSN 0022-4928, 1520-0469. doi: 10.1175/JAS-D-10-05024.1.
- Emanuel, K., Ravela, S., Vivant, E., and Risi, C. A Statistical Deterministic Approach to Hurricane Risk Assessment. *Bulletin of the American Meteorological Society*, 87(3):299–314, March 2006. ISSN 0003-0007, 1520-0477. doi: 10.1175/BAMS-87-3-299. URL <https://journals.ametsoc.org/view/journals/bams/87/3/bams-87-3-299.xml>. Publisher: American Meteorological Society Section: Bulletin of the American Meteorological Society.
- Emmert-Streib, F., Yang, Z., Feng, H., Tripathi, S., and Dehmer, M. An introductory review of deep learning for prediction models with big data. *Frontiers in Artificial Intelligence*, 3:4, 2020. Publisher: Frontiers Media SA.
- Gori, A., Lin, N., Xi, D., and Emanuel, K. Tropical cyclone climatology change greatly exacerbates US extreme rainfall–surge hazard. *Nature Climate Change*, 12(2):171–178, February 2022. ISSN 1758-6798. doi: 10.1038/s41558-021-01272-7. URL <https://www.nature.com/articles/s41558-021-01272-7>. Publisher: Nature Publishing Group.
- Group, U. Final Coastal and Riverine High Water Mark Collection for Hurricane Katrina in Mississippi. Technical report, March 2006a. URL https://www.fema.gov/pdf/hazard/flood/recoverydata/katrina/katrina_ms_hwm_public.pdf.

- Group, U. High Water Mark Collection for Hurricane Katrina in Alabama. Technical report, April 2006b. URL https://www.fema.gov/pdf/hazard/flood/recoverydata/katrina/katrina_ms_hwm_public.pdf.
- Group, U. High Water Mark Collection for Hurricane Katrina in Louisiana. Technical report, March 2006c. URL https://www.fema.gov/pdf/hazard/flood/recoverydata/katrina/katrina_ms_hwm_public.pdf.
- Hochreiter, S. and Schmidhuber, J. Long short-term memory. *Neural computation*, 9(8):1735–1780, 1997. Publisher: MIT press.
- Holland, G. A Revised Hurricane Pressure–Wind Model. *Monthly Weather Review*, 136, September 2008. doi: 10.1175/2008MWR2395.1. URL <https://journals.ametsoc.org/view/journals/mwre/136/9/2008mwr2395.1.xml>.
- Islam, M. R., Lee, C.-Y., Mandli, K. T., and Takagi, H. A new tropical cyclone surge index incorporating the effects of coastal geometry, bathymetry and storm information. *Scientific Reports*, 11(1):16747, August 2021. ISSN 2045-2322. doi: 10.1038/s41598-021-95825-7. URL <https://www.nature.com/articles/s41598-021-95825-7>. Number: 1 Publisher: Nature Publishing Group.
- Islam, M. R., Satoh, M., and Takagi, H. Tropical Cyclones Affecting Japan Central Coast and Changing Storm Surge Hazard since 1980. *Journal of the Meteorological Society of Japan. Ser. II*, 100(3):493–507, 2022. doi: 10.2151/jmsj.2022-024.
- Jarvinen, B. R., Neumann, C. J., and Davis, M. A. S. A tropical cyclone data tape for the North Atlantic basin, 1886-1983 : contents, limitations, and uses. 1984. URL <https://repository.library.noaa.gov/view/noaa/7069/>.
- Kelly, P., Leung, L. R., Balaguru, K., Xu, W., Mapes, B., and Soden, B. Shape of Atlantic Tropical Cyclone Tracks and the Indian Monsoon. *Geophysical Research Letters*, 45(19):10,746–10,755, 2018. ISSN 1944-8007. doi: 10.1029/2018GL080098. URL <https://onlinelibrary.wiley.com/doi/abs/10.1029/2018GL080098>. eprint: <https://onlinelibrary.wiley.com/doi/pdf/10.1029/2018GL080098>.
- Kingma, D. P. and Ba, J. Adam: A method for stochastic optimization. *arXiv preprint arXiv:1412.6980*, 2014.
- Knapp, K. R., Kruk, M. C., Levinson, D. H., Diamond, H. J., and Neumann, C. J. The International Best Track Archive for Climate Stewardship (IBTrACS): Unifying Tropical Cyclone Data. *Bulletin of the American Meteorological Society*, 91(3):363–376, March 2010. ISSN 0003-0007, 1520-0477. doi: 10.1175/2009BAMS2755.1. URL https://journals.ametsoc.org/view/journals/bams/91/3/2009bams2755_1.xml. Publisher: American Meteorological Society Section: Bulletin of the American Meteorological Society.
- Knapp, K. R., Diamond, H. J., Kossin, J. P., Kruk, M. C., and Schreck, C. J. International Best Track Archive for Climate Stewardship (IBTrACS) Project, Version 4, North Atlantic, 2018.
- Knutson, T., Camargo, S. J., Chan, J. C. L., Emanuel, K., Ho, C.-H., Kossin, J., Mohapatra, M., Satoh, M., Sugi, M., Walsh, K., and Wu, L. Tropical Cyclones and Climate Change Assessment: Part II: Projected Response to Anthropogenic Warming. *Bulletin of the American Meteorological Society*, 101(3):E303–E322, March 2020. ISSN 0003-0007, 1520-0477. doi: 10.1175/BAMS-D-18-0194.1. URL <https://journals.ametsoc.org/view/journals/bams/101/3/bams-d-18-0194.1.xml>. Publisher: American Meteorological Society Section: Bulletin of the American Meteorological Society.
- LeCun, Y., Bengio, Y., and Hinton, G. Deep learning. *Nature*, 521(7553):436–444, May 2015. ISSN 1476-4687. doi: 10.1038/nature14539. URL <https://www.nature.com/articles/nature14539>. Bandiera_abtest: a Cg.type: Nature Research Journals Number: 7553 Primary_atype: Reviews Publisher: Nature Publishing Group Subject.term: Computer science;Mathematics and computing Subject_term.id: computer-science;mathematics-and-computing.

- Lipari, S., Balaguru, K., Rice, J., Feng, S., Xu, W., K. Berg, L., and Judi, D. Amplified threat of tropical cyclones to US offshore wind energy in a changing climate. *Communications Earth & Environment*, 5(1): 1–10, December 2024. ISSN 2662-4435. doi: 10.1038/s43247-024-01887-6. URL <https://www.nature.com/articles/s43247-024-01887-6>. Publisher: Nature Publishing Group.
- Luetlich, R. A., Westerink, J. J., and Scheffner, N. W. ADCIRC: an advanced three-dimensional circulation model for shelves, coasts, and estuaries. Report 1, Theory and methodology of ADCIRC-2DD1 and ADCIRC-3DL. 1992. Publisher: Coastal Engineering Research Center (US).
- Luetlich Jr., R. A. and Westerink, J. J. A solution for the vertical variation of stress, rather than velocity, in a three-dimensional circulation model. *International Journal for Numerical Methods in Fluids*, 12(10): 911–928, 1991. ISSN 1097-0363. doi: 10.1002/fld.1650121002.
- Marks, D. G. The Beta and advection model for hurricane track forecasting. 1992. URL <https://repository.library.noaa.gov/view/noaa/7184>.
- Martín Abadi, Ashish Agarwal, Paul Barham, Eugene Brevdo, Zhifeng Chen, Craig Citro, Greg S. Corrado, Andy Davis, Jeffrey Dean, Matthieu Devin, Sanjay Ghemawat, Ian Goodfellow, Andrew Harp, Geoffrey Irving, Michael Isard, Jia, Y., Rafal Jozefowicz, Lukasz Kaiser, Manjunath Kudlur, Josh Levenberg, Dandelion Mané, Rajat Monga, Sherry Moore, Derek Murray, Chris Olah, Mike Schuster, Jonathon Shlens, Benoit Steiner, Ilya Sutskever, Kunal Talwar, Paul Tucker, Vincent Vanhoucke, Vijay Vasudevan, Fernanda Viégas, Oriol Vinyals, Pete Warden, Martin Wattenberg, Martin Wicke, Yuan Yu, and Xiaoqiang Zheng. TensorFlow: Large-Scale Machine Learning on Heterogeneous Systems, 2015. URL <https://www.tensorflow.org/>.
- Muis, S., Aerts, J. C. J. H., Á. Antolínez, J. A., Dullaart, J. C., Duong, T. M., Erikson, L., Haarsma, R. J., Apecechea, M. I., Mengel, M., Le Bars, D., O’Neill, A., Ranasinghe, R., Roberts, M. J., Verlaan, M., Ward, P. J., and Yan, K. Global Projections of Storm Surges Using High-Resolution CMIP6 Climate Models. *Earth’s Future*, 11(9):e2023EF003479, 2023. ISSN 2328-4277. doi: 10.1029/2023EF003479. URL <https://onlinelibrary.wiley.com/doi/abs/10.1029/2023EF003479>. eprint: <https://onlinelibrary.wiley.com/doi/pdf/10.1029/2023EF003479>.
- Murakami, H. and Wang, B. Patterns and frequency of projected future tropical cyclone genesis are governed by dynamic effects. *Communications Earth & Environment*, 3(1):1–10, April 2022. ISSN 2662-4435. doi: 10.1038/s43247-022-00410-z. URL <https://www.nature.com/articles/s43247-022-00410-z>. Publisher: Nature Publishing Group.
- Needham, H. *A Data-Driven Storm Surge Analysis for the U.S. Gulf Coast*. Doctor of Philosophy, Louisiana State University and Agricultural and Mechanical College, March 2014. URL https://repository.lsu.edu/gradschool_dissertations/3250.
- Pringle, W. J., Wirasaet, D., Roberts, K. J., and Westerink, J. J. Global storm tide modeling with ADCIRC v55: unstructured mesh design and performance. *Geoscientific Model Development*, 14(2):1125–1145, February 2021. ISSN 1991-959X. doi: 10.5194/gmd-14-1125-2021. URL <https://gmd.copernicus.org/articles/14/1125/2021/>. Publisher: Copernicus GmbH.
- Rice, J. R., Balaguru, K., Staid, A., Xu, W., and Judi, D. Projected increases in tropical cyclone-induced U.S. electric power outage risk. *Environmental Research Letters*, 20(3):034030, February 2025. ISSN 1748-9326. doi: 10.1088/1748-9326/adad85. URL <https://dx.doi.org/10.1088/1748-9326/adad85>. Publisher: IOP Publishing.
- Vafeidis, A. T., Schuerch, M., Wolff, C., Spencer, T., Merkens, J. L., Hinkel, J., Lincke, D., Brown, S., and Nicholls, R. J. Water-level attenuation in global-scale assessments of exposure to coastal flooding: a sensitivity analysis. *Natural Hazards and Earth System Sciences*, 19(5):973–984, May 2019. ISSN 1561-8633. doi: 10.5194/nhess-19-973-2019. URL <https://nhess.copernicus.org/articles/19/973/2019/>. Publisher: Copernicus GmbH.

- Willoughby, H. E., Darling, R. W. R., and Rahn, M. E. Parametric Representation of the Primary Hurricane Vortex. Part II: A New Family of Sectionally Continuous Profiles. *Monthly Weather Review*, 134, April 2006. doi: 10.1175/MWR3106.1. URL <https://journals.ametsoc.org/view/journals/mwre/134/4/mwr3106.1.xml>.
- Xu, W., Balaguru, K., August, A., Lalo, N., Hodas, N., DeMaria, M., and Judi, D. Deep Learning Experiments for Tropical Cyclone Intensity Forecasts. *Weather and Forecasting*, 36(4):1453–1470, August 2021. ISSN 1520-0434, 0882-8156. doi: 10.1175/WAF-D-20-0104.1. URL <https://journals.ametsoc.org/view/journals/wefo/36/4/WAF-D-20-0104.1.xml>. Publisher: American Meteorological Society Section: Weather and Forecasting.
- Xu, W., Balaguru, K., Judi, D. R., Rice, J., Leung, L. R., and Lipari, S. A North Atlantic synthetic tropical cyclone track, intensity, and rainfall dataset. *Scientific Data*, 11(1):130, January 2024. ISSN 2052-4463. doi: 10.1038/s41597-024-02952-7. URL <https://www.nature.com/articles/s41597-024-02952-7>. Number: 1 Publisher: Nature Publishing Group.